Cryptoclidus eurymerus humerus and femur finite element structure analyses inform on plesiosaur muscle forces and flipper twisting (#58478)

First submission

Guidance from your Editor

Please submit by **6 Apr 2021** for the benefit of the authors (and your $200 publishing discount) .

Structure and Criteria
Please read the 'Structure and Criteria' page for general guidance.

Author notes
Have you read the author notes on the guidance page?

Raw data check
Review the raw data.

Image check
Check that figures and images have not been inappropriately manipulated.

Privacy reminder: If uploading an annotated PDF, remove identifiable information to remain anonymous.

Files
Download and review all files from the materials page.

7 Figure file(s)
5 Table file(s)
2 Raw data file(s)

Structure and Criteria

Structure your review

The review form is divided into 5 sections. Please consider these when composing your review:

1. **BASIC REPORTING**
2. **EXPERIMENTAL DESIGN**
3. **VALIDITY OF THE FINDINGS**
4. General comments
5. Confidential notes to the editor

You can also annotate this PDF and upload it as part of your review

When ready submit online.

Editorial Criteria

Use these criteria points to structure your review. The full detailed editorial criteria is on your guidance page.

BASIC REPORTING

- Clear, unambiguous, professional English language used throughout.
- Intro & background to show context. Literature well referenced & relevant.
- Structure conforms to PeerJ standards, discipline norm, or improved for clarity.
- Figures are relevant, high quality, well labelled & described.
- Raw data supplied (see PeerJ policy).

EXPERIMENTAL DESIGN

- Original primary research within Scope of the journal.
- Research question well defined, relevant & meaningful. It is stated how the research fills an identified knowledge gap.
- Rigorous investigation performed to a high technical & ethical standard.
- Methods described with sufficient detail & information to replicate.

VALIDITY OF THE FINDINGS

- Impact and novelty not assessed. Negative/inconclusive results accepted. *Meaningful* replication encouraged where rationale & benefit to literature is clearly stated.
- All underlying data have been provided; they are robust, statistically sound, & controlled.
- Speculation is welcome, but should be identified as such.
- Conclusions are well stated, linked to original research question & limited to supporting results.

Standout reviewing tips

The best reviewers use these techniques

Tip	*Example*
Support criticisms with evidence from the text or from other sources	*Smith et al (J of Methodology, 2005, V3, pp 123) have shown that the analysis you use in Lines 241-250 is not the most appropriate for this situation. Please explain why you used this method.*
Give specific suggestions on how to improve the manuscript	*Your introduction needs more detail. I suggest that you improve the description at lines 57- 86 to provide more justification for your study (specifically, you should expand upon the knowledge gap being filled).*
Comment on language and grammar issues	*The English language should be improved to ensure that an international audience can clearly understand your text. Some examples where the language could be improved include lines 23, 77, 121, 128 – the current phrasing makes comprehension difficult. I suggest you have a colleague who is proficient in English and familiar with the subject matter review your manuscript, or contact a professional editing service.*
Organize by importance of the issues, and number your points	*1. Your most important issue* *2. The next most important item* *3. …* *4. The least important points*
Please provide constructive criticism, and avoid personal opinions	*I thank you for providing the raw data, however your supplemental files need more descriptive metadata identifiers to be useful to future readers. Although your results are compelling, the data analysis should be improved in the following ways: AA, BB, CC*
Comment on strengths (as well as weaknesses) of the manuscript	*I commend the authors for their extensive data set, compiled over many years of detailed fieldwork. In addition, the manuscript is clearly written in professional, unambiguous language. If there is a weakness, it is in the statistical analysis (as I have noted above) which should be improved upon before Acceptance.*

Cryptoclidus eurymerus humerus and femur finite element structure analyses inform on plesiosaur muscle forces and flipper twisting

Anna Krahl Corresp., [1, 2, 3], **Andreas Lipphaus** [1], **Paul Martin Sander** [3], **Ulrich Witzel** [1]

[1] Biomechanics Research Group, Chair of Product Development, Faculty of Mechanical Engineering, Universitätsstr. 150, Ruhr-Universität Bochum, 44801 Bochum, Germany

[2] Fachbereich Geowissenschaften, Hölderlinstraße 12, Eberhard-Karls-Universität Tübingen, 72074 Tübingen, Germany

[3] Institute of Geoscience, Section Paleontology, Nußallee 8, Rheinische Friedrich-Wilhelms Universität Bonn, 53115 Bonn, Germany

Corresponding Author: Anna Krahl
Email address: annakrahl1@googlemail.com

Background. Plesiosauria (Sauropterygia) are secondarily marine Diapsida. They are the only tetrapods that evolved hydrofoil fore- and hindflippers. Once this locomotory specialization had evolved, it remained essentially unchanged for 135 Ma. It is still contentious whether plesiosaurs flew underwater, rowed, or employed a mixture of both styles. Long bones of Tetrapoda experience torsion, bending, and compression during locomotion. Load case superposition indicates that bones are loaded primarily by compression. Thus, it is possible to use finite element analyses as a test environment for hypotheses of muscle lines of action (LOA), if the objective is to receive a homogenous compressive stress distribution and to optimize for bending minimization. **Methods.** To study locomotion in plesiosaurs, a *Cryptoclidus eurymerus* (Middle Jurassic Oxford Clay of the UK) humerus and femur were analyzed with FE methods according to this concept. Based on muscle reconstructions that had been undertaken earlier, LOA were deduced experimentally for all humerus and femur muscles of *Cryptoclidus*. These were acquired by spanning threads into a cast of a fore- and hindflipper of a mounted skeleton. LOA and muscle attachments were conveyed to a meshed volumetric model of the humerus and femur that were created from micro-CT scans. By computing the compressive stress distribution for two load cases, down- and upstroke, for each bone, muscle forces were approximated by stochastic iteration. **Results.** After the reconstruction of a flipper twisting mechanism driven by muscles and the addition of those extensors and flexors in the finite element models that originate from humerus and femur and contribute to flipper twisting, a homogenous compressive stress distribution was obtained. Humeral and femoral elevators and depressors, powering underwater flight and not rowing, were found to have the highest muscle forces. Extensors and flexors exert high muscle forces in comparison to Cheloniidae. This corroborates a myological flipper twisting mechanism in plesiosaurs complementing hydrodynamic studies that showed that flipper twisting is crucial for plesiosaur underwater flight.

Cryptoclidus eurymerus humerus and femur finite element structure analyses inform on plesiosaur muscle forces and flipper twisting

Anna Krahl[1,2], Andreas Lipphaus[1], Paul Martin Sander[3], Ulrich Witzel[1]

[1] Biomechanics Research Group, Chair of Product Development, Faculty of Mechanical Engineering, Ruhr-University Bochum, Universitätsstr. 150, 44801 Bochum, Germany
[2] Fachbereich Geowissenschaften an der Eberhard-Karls-Universität Tübingen, Hölderlinstraße 12, D-72074 Tübingen
[3] Institute of Geoscience, Section of Paleontology, Rheinische Friedrich-Wilhelms Universität Bonn, Nußallee 8, 53115 Bonn, Germany

Corresponding Author:
Anna Krahl[1]
Email address: anna.krahl@uni-tuebingen.de

Abstract

Background. Plesiosauria (Sauropterygia) are secondarily marine Diapsida. They are the only tetrapods that evolved hydrofoil fore- and hindflippers. Once this locomotory specialization had evolved, it remained essentially unchanged for 135 Ma. It is still contentious whether plesiosaurs flew underwater, rowed, or employed a mixture of both styles. Long bones of Tetrapoda experience torsion, bending, and compression during locomotion. Load case superposition indicates that bones are loaded primarily by compression. Thus, it is possible to use finite element analyses as a test environment for hypotheses of muscle lines of action (LOA), if the objective is to receive a homogenous compressive stress distribution and to optimize for bending minimization.

Methods. To study locomotion in plesiosaurs, a *Cryptoclidus eurymerus* (Middle Jurassic Oxford Clay of the UK) humerus and femur were analyzed with FE methods according to this concept. Based on muscle reconstructions that had been undertaken earlier, LOA were deduced experimentally for all humerus and femur muscles of *Cryptoclidus*. These were acquired by spanning threads into a cast of a fore- and hindflipper of a mounted skeleton. LOA and muscle attachments were conveyed to a meshed volumetric model of the humerus and femur that were created from micro-CT scans. By computing the compressive stress distribution for two load cases, down- and upstroke, for each bone, muscle forces were approximated by stochastic iteration.

Results. After the reconstruction of a flipper twisting mechanism driven by muscles and the addition of these extensors and flexors in the finite element models that originate from humerus

and femur and contribute to flipper twisting, a homogenous compressive stress distribution was obtained. Humeral and femoral elevators and depressors, powering underwater flight and not rowing, were found to have the highest muscle forces. Extensors and flexors exert high muscle forces in comparison to Cheloniidae. This corroborates a myological flipper twisting mechanism in plesiosaurs complementing hydrodynamic studies that showed that flipper twisting is crucial for plesiosaur underwater flight.

Introduction

Plesiosaur musculoskeletal apparatus and locomotion

Cryptoclidus eurymerus osteology

Plesiosauria are secondarily aquatic Tetrapoda that roamed the marine realm from the Late Triassic (Wintrich et al., 2017) until the K/Pg mass extinction (Bardet, 1994; Motani, 2009; Vincent et al., 2011; Vincent et al., 2013; Bardet et al., 2014). Plesiosauria form the most derived group of Sauropterygia. The origin of Sauropterygia remains obscure. They could have evolved from basal archosauromorphs (Merck, 1997) or lepidosauromorphs (Rieppel & Reisz, 1999), or they may be the sister taxon to archosauromorphs and lepidosauromorphs (Neenan, Klein & Scheyer, 2013). The most striking and unique key innovation of plesiosaurs is that they have evolved four similarly looking wing-like flippers by the Late Triassic (Wintrich et al., 2017). All four flippers are dorsoventrally flattened, have greatly foreshortened zeugopodium (< one-third of autopodium length), and form a hydrofoil (Robinson, 1975, 1977). They possibly had an asymmetrical profile (Robinson, 1975; Caldwell, 1997) like the flippers of recent underwater-flying Spheniscidae and Chelonioidea. Unlike plesiosaurs, Spheniscidae, Chelonioidea, Cetacea, and Otariinae have only evolved hydrofoil-like foreflippers (Walker, 1973; Schreiweis, 1982; Feldkamp, 1987; Fish & Battle, 1995; Fish, 2004; Cooper et al., 2007; Elliott et al., 2013). Sea turtle, penguin, and sea lion hindflippers evolved into paddles (Shufeldt, 1901; Walker, 1971b; Davenport, Munks & Oxford, 1984) and are employed in steering and terrestrial and aquatic locomotion (Walker, 1971b; Pinshow, Fedak & Schmidt-Nielsen, 1977; Clark & Bemis, 1979; Davenport, Munks & Oxford, 1984; Feldkamp, 1987; Wyneken, 1997). Whale hindlimbs are almost entirely reduced. Scapula, coracoid, pubis, and ischium of plesiosaurs lie ventrally and meet the element from the other side in the body midline in a slightly v-shaped configuration. Coracoid and pubis are much expanded. The dorsal expansion of the scapula and the dorsally directed ilium are much reduced (Andrews, 1910). Gastralia lie in between the pectoral and the pelvic girdle and stiffen the trunk region (Sues, 1987; Taylor, 1989). Humeri and femora of *Cryptoclidus eurymerus* have a round proximal end, an oval midshaft cross section, and the epicondyles are expanded and hammer-shaped (Andrews, 1910; personal observation on IPB R324, a *Cryptoclidus eurymerus* exhibit (Oxford Clay, Middle Jurassic, UK) at the Goldfuß Museum, Rheinische Friedrich-Wilhelms-Universität Bonn).

The distal expansion of the humerus of *Cryptoclidus* is larger than that of the femur and rather untypical for most plesiosaurs (compare to e.g., Großmann, 2006, Sachs, Hornung & Kear, 2016). Radius/ulna, and tibia/fibula are much shortened and rather disc-like in appearance

(Andrews, 1910). Metacarpal V and metatarsal V have been moved proximally into the rows of carpals and tarsals (Robinson, 1975). Fore- and hindflippers are hyperphalangic (Andrews, 1910).

Plesiosaur muscle reconstructions

Plesiosaur muscles have been reconstructed by Watson (1924), Tarlo (1958), Robinson (1975), Lingham-Soliar (2000), Carpenter et al. (2010), Araújo & Correia (2015), and by Krahl (2020). Carpenter et al. (2010) Araújo & Correia (2015), and Krahl (2020) relied on the extant phylogenetic bracket (EPB), a method that emerged in the 1990s which provides reliable inferences for soft tissue anatomy of fossils (Bryant & Russel, 1992; Wittmer, 1995). Older studies (Watson, 1924; Tarlo, 1958; Robinson, 1975; Lingham-Soliar, 2000) did not employ the EPB and did not clearly state which extant taxa they relied on for their muscle reconstructions. Muscles that originate on the pectoral girdle and insert into the humerus or span it have been reconstructed by Watson (1924), Tarlo (1958), Robinson (1975), Lingham-Soliar (2000), Carpenter et al. (2010), Araújo & Correia (2015), and by Krahl (2020). Locomotor muscles which arise from the pelvic girdle, traverse the femur, and attach to the femur have been partially reconstructed by Robinson (1975), Lingham-Soliar (2000), and Carpenter et al. (2010) and completely by Krahl (2020). Muscles which arise distally from the humerus and femur have been partially reconstructed by Robinson (1975) and entirely by Krahl (2020). Robinson (1975) seems to have reconstructed the ventral side of the foreflipper and the dorsal side of the hindflipper although thus is not clearly stated (Robinson, 1975; Krahl, 2020). The possible implication is that the dorsal and ventral fore- and hindflipper sides could look the same in plesiosaurs is unsubstantiated by the EPB, as dorsal and ventral fore- and hindlimb musculature of extant Sauropsida is not symmetrical (Walker, 1973; Meers, 2003; Russell & Bauer, 2008; Suzuki et al., 2011). The distal plesiosaur fore- and hindflipper musculature reconstructed by Robinson (1975) looks very similar to the cetacean foreflipper musculature in terms of how extremely reduced it is (Cooper et al., 2007). This whale-like state appears unlikely for plesiosaurs, as cetacean foreflippers are merely control surfaces and not hydrofoils (Fish, 2002; Woodward, Winn & Fish, 2006) while the main propulsive organ of whales is a large muscular swimming tail with a fluke (Fish, 1996; Woodward, Winn & Fish, 2006). Contrastingly, plesiosaurs actively swam with their fore- and hindflippers (Krahl, 2020). Krahl (2020) are the first who reconstructed the entire locomotor musculature of a plesiosaur fore- and hindflipper. They reconstructed a complex array of muscles for fore- and hindflipper of plesiosaurs which enables the plesiosaur to twist both its flipper pairs along the flipper length and maybe even actively control the flipper profile, as hydrodynamic computations of plesiosaurs by Witzel, Krahl & Sander (2015) and Witzel (2020) suggest.

Plesiosaur locomotion

The locomotory style of plesiosaurs has been an ongoing debate since over one century (Williston, 1914; Watson, 1924; Tarlo, 1958; Robinson, 1975, 1977; Feldkamp, 1987; Lingham-

Soliar, 2000; Carpenter et al., 2010; Araújo et al., 2015; Araújo & Correia, 2015; Liu et al., 2015; Krahl, 2020). It has been suggested that plesiosaurs row like ducks or otters (Williston, 1914; Watson, 1924; Tarlo, 1958; Araújo et al., 2015; Araújo & Correia, 2015), fly underwater like sea turtles and penguins (Robinson, 1975, 1977; Lingham-Soliar, 2000; Carpenter et al., 2010; Liu et al., 2015; Krahl, 2020), or use rowing-flight like sea lions (Feldkamp, 1987; Liu et al., 2015). The main difference between the different locomotory styles results from the underlying hydrodynamics: In rowing, water drag is used to push the body forward while in underwater flight, lift produced by the onflowing water travelling around a cambered flipper profile is used (e.g., Baudinette & Gill, 1985; Fish, 1996; Walker & Westneat, 2000). The rowing-flight of sea lions relies on both hydrodynamic mechanisms, drag-based and lift-based, at different phases of the limb cycle (Feldkamp, 1987). It was also proposed that the foreflipper pairs employ a different mode of locomotion (Tarlo, 1958; Lingham-Soliar, 2000; Liu et al., 2015).

A flipper used in rowing is mostly moved in anteroposterior direction with little dorsoventral motion (Pace, Blob & Westneat, 2001; Rivera, Rivera & Blob, 2011; Rivera, Rivera & Blob, 2013). The anteroposterior expansion and the dorsoventral reduction of the bony elements of the plesiosaur pectoral and pelvic girdle, as well as the accompanying reduction or hypertrophy of locomotory muscles have been interpreted as being in favor for protraction and retraction of the flipper, i.e., a rowing motion (Watson, 1924; Tarlo, 1958; Godfrey, 1984).

Contrastingly, during underwater flight, the flipper is beaten mainly in dorsoventral direction with a minor anteroposterior component. The flipper downstroke of Chelonioidea and Spheniscidae is characterized by major depression and minor retraction of the flipper. The upstroke is performed by humeral elevation and protraction. The flipper tip describes a skewed “O” in anterodorsal-posteroventral direction (Clark & Bemis, 1979; Davenport, Munks & Oxford, 1984; Rivera, Wyneken & Blob, 2011; Rivera, Rivera & Blob, 2013). As Robinson (1975) noted, the hydrofoil-shaped flippers of plesiosaurs, tapering towards the tip, superficially comparable to that of penguins and sea turtles, imply that they were used for underwater flight and not for rowing. Also, the glenoid and acetabular shape of plesiosaurs restrict movement in anteroposterior direction more than in dorsoventral direction (Krahl, 2020).

During rowing flight, the downstroke is lift-generating and similar to the downstroke of the underwater fliers. At the point of maximum flipper depression, the flipper is turned around like a paddle and pushes against the water during its retraction and elevation. During the recovery stroke, the flipper is brought back anteriorly and dorsally, possibly also producing propulsion by lift (Feldkamp, 1987). Godfrey (1984) found that in recent underwater fliers, the shoulder girdles are characterized by a strong bony support expanding in the dorsoventral direction, which is not present in plesiosaurs. Therefore, he noted that there is more similarity between sea lions and plesiosaurs than with recent “true” underwater fliers (Godfrey, 1984).

Besides the locomotory style, it is still being discussed how the four flippers were moved in relation to each other, i.e., fore- and hindflipper synchronously, asynchronously, or out of phase. This debate is based on the so called four-wing problem which addresses how plesiosaurs avoided placing their hindflippers into the vortices shed by their foreflippers which would mean a considerable performance decrease of the hindflippers (Frey & Riess, 1982; Tarsitano & Riess, 1982; Lingham-Soliar, 2000; Carpenter et al., 2010; Muscutt et al., 2017).

Muscle physiology

During a limb motion cycle, muscles may follow either a shortening-stretch cycle or a stretch-shortening cycle. During the former, the muscle is shortened while its force output increases. Then, the muscle is stretched and the force output decreases. During the latter, the muscle is stretched at the beginning while its force output increases. When the muscle contracts, its force output drops (Rassier, MacIntosh & Herzog, 1999). Muscle force production depends on muscle architecture. Muscle architecture includes muscle length and tendon (if present) length, lines of action, muscle mass, specific density of muscle, intrinsic muscle strength, fascicle length, and pennation angles (Alexander & Vernon, 1975; Gans, 1982; Sacks & Roy, 1982; Powell et al., 1984; Narici, Landoni & Minetti, 1992; Anapol & Barry, 1996; Kummer, 2005; Azizi, Brainerd & Roberts, 2008). Parallel-fibred muscles have on average longer fascicles, a larger volume, and can contract faster (which depends on the fibre type composition) than pennate muscles. However, more muscle fibres can be arranged adjacently to each other in a pennate muscle than in a parallel-fibred muscle of the same size. Thus, a pennate muscle can exert a higher force than a same-sized parallel-fibred muscle, although the pennate muscle has shorter fibres. This is so because the exerted maximum muscle force does not only depend on the fibre length but also on the physiological cross sectional area (PCSA), i.e., the sum of fibre cross sections (Gans, 1982; Burkholder et al., 1994; Allen et al., 2010; Huq, Wall & Taylor, 2015).

Also, muscle length of a parallel-fibred, fast contracting muscle (or one close to it) varies substantially and is traded off for a high metabolic intake and a relatively low force production. Contrastingly, strongly pennated muscles exert relatively high forces at markedly lower metabolic costs but are much slower contracting and have poor fibre contraction control (Biewener & Roberts, 2000).

Pennate muscles may develop relatively high forces while their muscle lengths behave almost isometrically (e.g., turkey (musculus (m.) gastrocnemius) (Roberts et al., 1997) or wallaby (m. gastrocnemius, m. plantaris) (Biewener, Konieczynski & Baudinette, 1998). Contrastingly, the fan-shaped m. pectoralis, which has a very high initial power output, shows a very great muscle length change of 30-40% for *Columba liva* (Biewener, Corning & Tobalske, 1998; Biewener & Roberts, 2000) or approximately 30% for *Anas platyrhynchos* (Williamson, Dial & Biewener, 2001). Generally, muscle length change of vertebrate striated muscle may span up to +/- 25% (contraction and stretching in relation to resting length (=0%)) before its capability to generate force drops markedly (Biewener & Roberts, 2000).

Finite element structure analysis

As strain gauge measurements demonstrate, long bones of Tetrapoda are functionally loaded fluctuatingly by torsion, compression, and bending (Biewener & Dial, 1995; Carrano, 1998; Blob & Biewener, 1999; Lieberman, Polk & Demes, 2004; Main & Biewener, 2004, 2007; Butcher et al., 2008; Butcher & Blob, 2008; Sheffield et al., 2011; Young & Blob, 2015; Young et al., 2017). They are mostly loaded by bending in alternating directions or primarily by compression and subordinately by tension (Biewener & Dial, 1995; Blob & Biewener, 1999; Lieberman, Polk & Demes, 2004; Main & Biewener, 2004; Butcher et al., 2008; Butcher & Blob, 2008; Sheffield et al., 2011). High torsional loads are imposed on terrestrial tetrapod long bones (Biewener & Dial, 1995; Carrano, 1998; Blob & Biewener, 1999; Main & Biewener, 2004, 2007; Butcher et al., 2008; Butcher & Blob, 2008; Sheffield et al., 2011).

To reflect such changing loading conditions, a number of loadcases can be analyzed with finite element structure analysis (FESA; Witzel & Preuschoft, 2005) and then be superimposed on each other (Carter, Orr & Fyhrie, 1989). By reducing the bending moment (Klenner et al., 2015; Lutz et al., 2016; Milne, 2016; McCabe et al., 2017; Lipphaus & Witzel, 2018), biological lightweight structures may evolve (Klenner et al., 2015). FESA is used in different disciplines encompassing engineering sciences and biomechanics (Rayfield, 2007). FESA allows analysis of mechanical stresses and strains in technical and biological structures in 2-D or 3-D (Rayfield, 2007; Witzel et al., 2011) and may add to our understanding of the function of bony elements (Witzel et al., 2011). Compressive loads are applied to the bone via tension chords. Tension chords are either muscles (active tension chord) or ligaments (passive tension chords), and they act in pairs of agonists and antagonists (Witzel & Preuschoft, 2005; Sverdlova & Witzel, 2010; Curtis et al., 2011; Witzel et al., 2011; Klenner et al., 2015; Felsenthal & Zelzer, 2017). A movement is powered by the agonist while the antagonist opposes it to fulfill a controlled movement (Sverdlova & Witzel, 2010). If the same movement is inverted, the agonist becomes the antagonist and vice versa. Thus, agonists and antagonists load a bony structure constantly by compressive stress, although the agonist is exerting proportionally a higher force than the antagonist.

The aim of this study was to test plesiosaur muscle reconstructions with FESA. ~~So,~~ the muscle reconstructions obtained with the EPB, i.e., based on comparative anatomical studies, were cross-checked with the mechanically imposed demands on muscles. We evaluated how muscle physiological details, such as muscle length changes can contribute to muscle reconstructions of fossils and whether FESA of the plesiosaur humerus and femur can inform on plesiosaur locomotion. The results complement earlier hydrodynamic studies that implied that plesiosaurs must have used flipper twisting for efficient underwater flight (Witzel, Krahl & Sander, 2015; Witzel, 2020) and corroborate the myological flipper twisting mechanism reconstructed by Krahl (2020).

Materials & Methods

Analog model of lines of action

Lines of action (LOA) represent the direct connection in a straight line between a muscle's origin and insertion (Krahl et al., 2019). They were experimentally attained in an analog model (Figure 1) with the help of casts of the pectoral (Figure 2, 3) and pelvic girdle and limbs (Figure 4, 5) of the *Cryptoclidus eurymerus* specimen (IGPB R 324) on exhibition in the Goldfuß Museum, Division of Paleontology, Institute of Geosciences, Rheinische Friedrich-Wilhelms-Universität Bonn. The casts of the pectoral and pelvic girdle were mounted on a wooden frame and fixed with screws. In place of the vertebral column, which also serves as origin of locomotory muscles, wooden bars were screwed. The anatomical positioning of the casts and the vertebral column are based on the mounting of IGPB R 324. Thick styrofoam was used to replace the missing cartilage capping in the shoulder and hip joint. The fore- and hindflipper were hung into the construction and the respective joint with the help of the muscle lines of action. Supportively, the flippers were fixed by additional ropes in the chosen flipper positions (Figure 1).

To physically model the lines of action, non-elastic thread was used. Screw eye pins were screwed into the cast at the muscle origin and insertion surfaces. Muscle attachments of all locomotory muscles of the fore- and hindflipper that span either glenoid or acetabulum (12 on foreflipper, 14 on hindflipper) were adopted from Krahl (2020). Each thread was strung through three electrical terminal strips. Next, hooks were tied to both ends of the threads, which were then hooked into the screw eyes representing muscle origins and insertions (Figure 1). If a muscle attachment surface is small, the screw eye pin was screwed approximately in the middle of it. Contrastingly, muscles with large attachment areas were subdivided into several subportions to better encompass the varying fiber insertion angles and directions and to obtain more evenly distributed compressive stresses in the FE models. Correspondingly, the total muscle force of a muscle was subdivided, too, and fractions of the total muscle force were assigned to the subportions. Usually, the most anterior and posterior points in the body midline were chosen for placement of the screw eye pins (e.g., m. subcoracoscapularis, m. coracobrachialis brevis, m. pectoralis). In the case of, e.g., m. latissimus dorsi, a position in between the cranialmost and caudalmost origin was chosen. This is done in order to represent those portions that are supported the best by EPB (cranial and middle portion) but also to cover the less well supported portion (caudal) (Krahl, 2020).

These subportions do not necessarily represent actual partitions of the reconstructed muscles, although some muscles may have likely been compartementalized, e.g., m. pectoralis, m. latissimus dorsi, m. puboischiofemoralis internus, and m. puboischiofemoralis externus. Muscles with two or more heads (i.e., m. deltoideus scapularis, m. deltoideus clavicularis, m. coracobrachialis brevis, m. coracobrachialis longus, m. triceps brachii, m. caudifemoralis brevis (ilium and vertebral column), m. flexor tibialis internus, m. flexor tibialis externus, m. puboischiofemoralis internus, and m. puboischiofemoralis externus were assigned two (or more) threads. The resultant vector of the various subportions of those muscles that have a large origin area went into the FE models. Agonistically and antagonistically acting muscles that insert into, originate from, or span the humerus (Table 2) and femur (Table 3) were devised from the mount. Pictures were taken for documentation from cranial/anterior (Figure 2 a-f; Figure 4 a-f), caudal/posterior (Figure 3 a-f; Figure 5 a-f), ventral (Figure 2 g, h; Figure 4 g, h) and dorsal (Figure 3 g, h; Fig 5 g, h). In Figure 2 g) and h), Figure 3 g) and h), Figure 4 b), g), and h), and

Figure 5 g), h) some muscles are pictured that do not run relatively close to either humerus, femur, or the flipper. This is due to measuring muscle length changes in the analog model. The FESA are based on sketches in which we presumed force vectors for the respective muscles that were on average lying closer to the adjacent bony elements. These muscles were possibly held close by annular pulleys. Limb cycle movement terminology follows Rivera, Wyneken & Blob (2011) and Krahl (2020) who used humeral and femoral depression, elevation, protraction, and retraction, which reflect the requirements for underwater flight well.

Changes in muscle length

Three positions in the fore- and hindflipper beat cycle were chosen to measure the total muscle length change for muscles that originate on the pectoral and pelvic girdle or the vertebrae and insert into or span the humerus and femur. These positions are the maximum dorsal excursion of the fore-/hindflipper during the upstroke (~ +50° to the horizontal) (Figure 2 a, b; Figure 3 a, b; Figure 4 a, b; Figure 5 a, b), maximum ventral excursion of the fore-/hindflipper during the downstroke (~ -50°) (Figure 2 e, f; Figure 3 e, f; Figure 4 e, f; Figure 5 e, f), and the neutral position (0°) (Figure 2 c, d; Figure 3 c, d; Figure 4 c, d; Figure 5 c, d). Based on the orientation of glenoid and acetabulum, the tip of the foreflipper points slightly forward, the hindflipper tip points slightly backward. Protraction and retraction were not considered because, based on the osteology, they contribute minorly to the flipper beat cycle. Also, in this study we examined basically whether or not total muscle length changes may add value for muscle reconstructions of extinct vertebrates.

Flipper range of motion has been determined before by Carpenter et al. (2010) and Liu et al. (2015) for various plesiosaur species, but the results depend greatly on how much cartilage is presumed to have been capping the humerus and femur and the glenoid and acetabulum, as indicated by Liu et al. (2015), and on the species (which differ in size of the dorsal tuberosity/trochanter). The authors presumed that the humeral and femoral head of *Cryptoclidus* (IGPB R 324) were capped by thick vascularized cartilage comparable to that described for *Dermochelys coriacea* (Rhodin, Ogden & Conlogue, 1981; Snover & Rhodin, 2008). This is based on the observation that the proximal bone surfaces of both, the humerus and femur of *Cryptoclidus* (IGPB R 324), are pierced by large vascular canals and are very similar looking to the proximal humeral head of *Dermochelys* (Rhodin, Ogden & Conlogue, 1981; Snover & Rhodin, 2008; Krahl, 2020.

The authors refrained from calling the neutral flipper position the resting position of the flipper because it is probably impossible to determine the flipper resting position for an extinct species. Furthermore, in the muscle physiological literature, the term „resting length“ usually refers to individual sarcomeres (Rassier, MacIntosh & Herzog, 1999) or fascicles of a muscle (Biewener & Roberts, 2000). Moreover, not to know the exact flipper resting length influences the exact value of muscle stretching and contraction but not the end result of total length change of a muscle which was calculated in this study (s. below). This is because the absolute values of muscle stretching and contraction are measured in relation to the neutral position but the total muscle length change is the difference between maximum muscle stretching and contraction.

All three positions of the fore- and hindflipper were successively fixed with ropes suspended from the wooden frame holding the casts. For each of the three states, the optimal length of each muscle was fixed with the help of the terminal strips. Afterwards, each muscle was removed and all three muscle lengths, i.e., maximum excursion during downstroke, neutral position, and maximum excursion during downstroke were measured with a measuring tape in cm. Length changes between maximum excursion at downstroke and the neutral position as well as between maximum excursion at upstroke and the neutral position were expressed first in cm and then in %, by setting resting length as 100%. Next, muscle stretching, muscle contraction, and the difference between both, the total length change of muscle, were calculated in % (Table 1). Bar graphs for total muscle length changes in % were plotted with Microsoft Excel (Figure 6 b). Some muscle length changes were recorded as 0 cm because the actual changes in length could not be measured because they were smaller than the width of the terminal strips. In one case, i.e., m. deltoideus scapularis, it was found that the total muscle length change with an insertion on the lateral scapula blade was unphysiologic (see below), another origin area (from the ventrolateral scapula) was tested and shown to give physiologically plausible results that were then measured for all three positions.

FESA and muscle force determination by computation

The right humerus and left femur of IGPB R 324 were scanned with the micro-CT scanner at the author's institution with an industrial high-resolution computed tomography (µCT) scanner (model phoenix v|tome|x s 240, produced by General Electric Phoenix X-ray, Wunstorf, Germany). The scans were processed with the dedicated software datos|x and the program VGStudio MAX (Volume Graphics) to obtain image stacks in the z direction.

The image stack was loaded into Simpleware ScanIP 5.1 (Krahl et al., 2019) for further processing. For each image, the bone tissue was selected and segmented out with the help of grey scale intervals and a model was generated (Data S1 and Data S2). Next, the model was imported into ANSYS 16.0 (ANSYS Inc., Canonsberg, PA, USA). The measured dimensions of the humerus and femur of IGPB R 324 were used to scale the respective volumetric model. Next, proximal articular cartilage, respectively the glenoid/acetabular articulation surface, were modelled. The FE models were created with the element type SOLID92. The humerus model consists of 92665 elements and the femur model of 75784 elements. In the humerus, the cartilaginous articular structure is formed by 19927 elements and by 15472 elements in the femur. Bearings were placed on all nodes of the proximal surface of the cartilage models for a different research project which will not be addressed further in the current study. In both FE models, bone was modelled with a Young's modulus of 12000 MPa and cartilage with a Young's modulus of 5 MPa.

LOA and attachment angles were figured in sketches of humerus (Figure 7 a) and femur (Fig, 7 e) in anterior, posterior, dorsal, and ventral view that were implemented in the FE models as vectors (Figure 7 b, f). Two- or more headed muscle bellies were entered in the FE model in form of the resultant vector. Two-joint muscles add to the counterforce. Radius and ulna/tibia and fibula exert the counterforce on the epicondyles of the humerus and femur. Two-joint muscles of the foreflipper are the m. triceps brachii and the m. biceps brachii. Two-joint muscles of the hindflipper are the m. ambiens, m. pubotibialis, m. flexor tibialis externus, m. flexor tibialis internus, m. iliotibialis, m. iliofibularis, and m. puboischiotibialis. As it is impossible to perform curved vectors in ANSYS 16.0., muscle wrappings were modelled by dividing their lines of action into several smaller straight vectors.

The force transmission on the distal articular surfaces of humerus and femur due to muscular activity was first applied in one point. This resulted in very high localized stress peaks. Therefore, force transmission was split up into several application points scattered over the distal articulation surfaces to receive a more realistic simulation of the load transmission via a surface.

Forces of each humerus and femur muscle were approximated stochastically. The distribution of compressive stress was computed for both long bones (Figure 7, c, d, g, h). Then, another run was prepared by maximizing compressive stresses and minimizing bending moments. These steps were repeated until a homogenous compressive stress distribution was obtained. This way, muscle forces were iteratively approximated (Table 3 and Table 4) (Witzel & Preuschoft, 2005; Sverdlova & Witzel, 2010).

Load case generation

Two load cases, downstroke and upstroke, were chosen to be computed to reflect the constantly varying loading regime of humerus and femur during the flipper beat cycle. For both load cases, a position was chosen in which the humerus is held horizontally at the level of the glenoid pointing laterally and slightly anteriorly, as indicated by the analog model. Similarly, the femur was positioned horizontally at the level of the acetabulum. Its flipper tip points mostly laterally but is also slightly angulated posteriorly. During the downstroke, the humerus and femur were rotated anteriorly downward along their long axis by approximately 19° (Witzel, Krahl & Sander, 2015; Witzel, 2020). During the upstroke, the humerus and femur were rotated back and about 19° posteriorly downward around their long axis (Witzel, Krahl & Sander, 2015; Witzel, 2020).

For the implementation of load cases, it is crucial to identify and consider which muscles act as agonists and antagonists (Witzel & Preuschoft, 2005). The shoulder and hip joint possibly allowed a minor clearance for rotation and protraction/retraction and a major clearance for elevation and depression stabilized by the interplay of agonists and antagonists. Muscle functions for identification of agonists and antagonists (Table 2 and Table 3) are taken from Krahl (2020). The downstroke load case is powered mainly by the humeral and femoral depressors, but also by retractors and those muscles enabling a slight downward rotation of the flipper leading edges. Flexors arising from the humerus and femur are active during the downstroke, flexing the digits and contributing to the twisting of the foreflipper and hindflipper along the flipper lengths. The upstroke load case is powered largely by humeral and femoral elevators. Humeral and femoral protraction and rotation of the flipper leading edge upward add to the upstroke as well. The extensors which originate from the distal humerus and femur aid in flipper twisting and extension of the digits during the upstroke (Krahl, 2020).

Results

Mechanically controlled plesiosaur muscle reconstructions

Humerus musculature

Humerus muscles that were reconstructed on a biological basis (Krahl and Witzel, 2020) are counterchecked for their functionality on a mechanical basis. Musculus deltoideus scapularis was reconstructed on the anteroventral scapula posterior to m. deltoideus clavicularis and anteriorly to m. supracoracoideus and on the lateral median scapular blade. Here we can confidently reject an origin from the blade, as a total muscle length change of 70% suggests extreme muscle shortening that it is physiologically impossible (see below) (Figure 6 a; Table 1).

Myological reconstruction suggests an m. biceps brachii origin on the posterior ventral coracoid. Musculus biceps brachii and m. brachialis could either insert via a shared tendon into the proximal radius or into the posteroproximal radius and the anteroproximal ulna. Further, m. triceps brachii originates anteriorly to anterodorsally from the bony ridge surrounding the glenoid on the scapula and from the coracoid just posterior to the glenoid and inserts (well substantiated by the EPB) into the posterodorsal ulna. The posterodorsal ulnar insertion of m. triceps brachii is unquestionable based on the EPB, and the posterior origin of m. biceps brachii is quite well supported as well. In contrast, origin areas of m. triceps brachii are debatable as well as the insertion area of m. biceps brachii and m. brachialis. This lead to interesting mechanical assumptions: our FESA was much improved when the m. biceps brachii/m. brachialis insertion was placed on the proximal and ventral radius and when the m. triceps brachii origin anterior to anterodorsally to the glenoid facet was more pronounced by a higher muscle force. An origin of the m. triceps brachii from the coracoid provides only a little to no lever arm and was therefore possibly reduced or lost.

Myological reconstruction suggests the insertions of m. coracobrachialis brevis and m. coracobrachialis longus due to the presence of osteological correlates on the posterior to posteroventral humeral shaft as observed in lepidosaurs (Russell & Bauer, 2008). This decision is not well supported by the EPB which would rather suggest an insertion ventrally into the intertrochanteric fossa as seen in turtles and crocodilians (Walker, 1973; Meers, 2003; Suzuki & Hayashi, 2010). A shift of their humeral insertions further distally along the shaft, is mechanically favorable as it increases the lever arms and took place comparably in Cheloniidae (Walker, 1973; Krahl et al., 2019).

Musculus scapulohumeralis anterior was not reconstructed based on myology because this muscle is only present in lepidosaurs and therefore weakly supported by EPB. However, we formulate a description and a reconstruction of this muscle below, because it adds a needed proximal rotatory component to the humeral locomotory musculature. Musculus scapulohumeralis anterior has no synonyms and is only reported for Lepidosauria (Russell &

Bauer, 2008). Musculus scapulohumeralis anterior has two portions which originate from the anterior ventrolateral scapula and from the posterolateral scapula, dorsal to the glenoid (in *Varanus exanthematicus*, *Iguana iguana*; Jenkins & Goslow, 1983; Russell & Bauer, 2008). For plesiosaurs, it is reconstructed to originate on the anterior edge of the lateral scapula, on the base of the scapular blade and on the posterior edge of the scapular blade. The lines of action support the latter origin because the former would result in a wrapping of m. scapulohumeralis anterior around the lateral scapular blade and around the musculature that suspends the pectoral girdle from the trunk, which seems rather unlikely. Yet, the origin on the posterior scapular blade would also only be able to support a very small muscle belly because the scapular blade is very much reduced in comparison to archosaurs, lepidosaurs, and turtles in general (Walker, 1973; Meers, 2003; Russell & Bauer, 2008; Suzuki & Hayashi, 2010). This means m. scapulohumeralis anterior is expected to contribute with a relatively low muscle force to propulsion. Musculus scapulohumeralis anterior inserts proximally and posterodorsally into the lepidosaur humerus, relatively proximally to the latissimus dorsi (Jenkins & Goslow, 1983; Russell & Bauer, 2008). Thus, a possible m. scapulohumeralis anterior insertion could be found proximally and posterodorsally, rather proximal to the m. latissimus dorsi insertion on the dorsal tuberosity of the *C. eurymerus* humerus associated with the strong rugosities on the dorsal humeral tuberosity.

Femur musculature

Femur muscle reconstructions followed biological principles and are counterchecked in the following chapter for their functionality. An m. ambiens origin site on the pubic tubercle is well supported by the EPB. An origin ventrally below the acetabulum would also be well substantiated by the EPB. From a mechanical point of view, the former has a much better lever arm than the latter, due to the rearrangement of pubis and ischium into almost ventrally flat lying plates. Therefore the m. ambiens origin site below the acetabulum can be rejected.

The m. iliofemoralis origin was reconstructed on the lateral ilium. Krahl (2020) also discuss a weakly supported option by EPB (only supported by turtles) that m. iliofemoralis origin area may have spread onto the vertebral column (Zug, 1971; Walker, 1973). An origin on the vertebral column would improve the lever arm of this muscle. Further, when the femur is depressed, m. iliofemoralis parallels and wraps around the dorsal trochanter of the femur and therefore exerts compressive stress onto it. The ilium is much reduced in size, comparable to the scapula blade. This would either indicate a much reduced ife or support its origin site shift onto the vertebral column which in turn would not limit its size in such a way.

Four origin areas are equally possible for m. puboischiofemoralis internus according to EPB: a large origin area on most of the dorsal pubis, a smaller origin on the anterodorsal ischium, a small origin area on the medial and ventral ilium, and an origin on the vertebral column. LOA of m. puboischiofemoralis internus show that they wrap around the dorsal trochanter of the plesiosaur femur. This means that m. puboischiofemoralis internus contributes substantially to femoral elevation. A large pubic portion and the ischiadic and vertebral column portion paralleling the dorsal trochanter can be substantiated from a mechanical standpoint. An iliac origin seems to be rather unlikely because it would wrap around the femoral trochanter and than around the anterior ilium. Then due to the reduction of the ilium, this portion can only be small. Further, total muscle shortening length shows this muscle has a bad performance. All of this indicates that an iliac origin of m. puboischiofemoralis internus is at least mechanically unlikely. The reconstructed iliac origin has a rather bad lever arm and shows no muscle shortening while the one from the vertebral column with a greater lever arm would be certainly favorable from a mechanical point of view.

M. gastrocnemius internus originating from the tibial epicondyle is equally well supported as an origin on the distal tibial epicondyle and the proximal tibia by EPB. FESA shows clearly that an origin similar to that of m. gastrocnemius externus, rather proximally on the tibial epicondyle at the point where the femur flairs anterodistally and posterodistally should be favored because otherwise it would be problematic to load the expanded femoral epicondyle by compressive stress in the FESA (see below).

Agonists and antagonists

Humerus musculature

Musculus coracobrachialis brevis, m. coracobrachialis longus, m. biceps brachii, the large posterior portions of m. pectoralis, m. subcoracoscapularis, m. supracoracoideus, and m. latissimus dorsi are humeral retractors. They oppose the humeral protractors which are m. deltoideus clavicularis, m. deltoideus scapularis, and the small anterior portions of m. supracoracoideus, m. subcoracoscapularis, and m. latissimus dorsi. Musculus deltoideus scapularis, m. subcoracoscapularis, m. latissimus dorsi and possibly to a very minor degree m. triceps brachii, m. scapulohumeralis anterior, and m. scapulohumeralis posterior power elevation of the humerus. The humeral depressors m. supracoracoideus, m. coracobrachialis brevis, m. coracobrachialis longus, m. deltoideus clavicularis, m. biceps brachii, and m. pectoralis act antagonistic to them. M. triceps brachii, the smaller anterior portion of m. subcoracoscapularis, the large posterior portion of m. pectoralis, m. biceps brachii, m. scapulohumeralis anterior, m. scapulohumeralis posterior, and m. deltoideus clavicularis contribute to downward rotation of the foreflipper leading edge. Functionally antagonistic are m. deltoideus scapularis, m. coracobrachialis brevis, m. corabcobrachialis longus, the larger posterior portion of m. subcoracoscapularis, and m. latissimus dorsi (Table 2).

Further sub-groupings of agonistic and antagonistic muscles are possible: The small anterior portion of m. latissimus dorsi (weak elevation and protraction) opposes the large posterior m. pectoralis portion (strong retraction and depression) in function. The small anteriorly lying m. pectoralis portion (protractor and depressor) and the large posterior m. latissimus dorsi portion (strong elevator and retractor) act as agonist and antagonist. Musculus subcoracoscapularis and m. deltoideus scapularis which elevate and protract the humerus find their functional antagonists in m. coracobrachialis brevis, m. coracobrachialis longus, m. biceps brachii, and the posterior portion of the m. supracoracoideus which depress and retract it. The large posterior portion of m. subcoracoscapularis acts as humeral elevator and retractor and the anterior portion of m. supracoracoideus and m. deltoideus clavicularis operate oppositional to them as humeral depressors and protractors (Table 2).

Muscles that originate from the humerus aid in flipper twisting (Krahl, 2020): Musculus flexor carpi ulnaris may offset the ulnar side of carpus relatively to the humerus ventrally (or flex metacarpal V) while m. extensor carpi ulnaris and humeral m. triceps brachii could both offset the ulna in the opposite direction and the former could possibly extend metacarpal V. Musculus flexor carpi radialis can either flex metacarpal I or offset the radial side of the plesiosaur carpus ventrally. Musculus brachialis, and m. pronator teres also contribute to the latter function. These are antagonistically matched by antagonistic m. supinator longus + m. extensor carpi radialis. M. flexor digitorum longus (flexion of digit I to V) is opposed by m. extensor digitorum communis and the digital extensors (extension of digits) (Table 2).

Femur musculature

Elevators of the hindflipper are m. puboischiofemoralis internus, m. iliotibialis, m. iliofemoralis, m. iliofibularis, m. caudifemoralis brevis, m. caudifemoralis longus, m. flexor tibialis externus (portion from ilium), m. flexor tibialis internus (portion from vertebral column). Musculus puboischiofemoralis externus, m. adductor femoris, m. ischiotrochantericus, m. puboischiotibialis, m. flexor tibialis externus (portion from ischium), and m. flexor tibialis internus (ischial portion) act as femoral depressors. Protractors are m. puboischiofemoralis externus (pubic portion), m. puboischiofemoralis internus (portion from pubis and from vertebral column), m. ambiens, and m. pubotibialis. Retractors of the hindflipper are m. puboischiofemoralis externus (ischial portion), m. puboischiofemoralis internus (ischial and iliac portion), m. adductor femoris, m. ischiotrochantericus, m. iliofemoralis, m. iliotibialis, m. iliofemoralis, m. caudifemoralis brevis, m. caudifemoralis longus, m. flexor tibialis externus, and m. flexor tibialis internus. Downward rotation of the flipper leading edge during the downstroke is enabled by the agonists, m. puboischiofemoralis internus (pubis portion), m. puboischiofemoralis externus (ischium portion), m. caudifemoralis brevis, m. caudifemoralis longus, m. ambiens (if femur elevated), m. ischiotrochantericus, m. iliofibularis (as long as fibula below origin), m. puboischiotibialis, m. pubotibialis (if femur elevated), m. flexor tibialis internus, and m. flexor tibialis externus. The agonists are opposed by the antagonistically acting m. iliotibialis, m. ambiens (if femur depressed), m. pubotibialis (if femur depressed), m. iliofemoralis, m. puboischiofemoralis internus (ischial and iliac portion small), and m. puboischiofemoralis externus (pubis portion large) (Table 3).

Further, the muscles can be assigned to the following subgroups: The m. puboischiofemoralis internus originating from the dorsal pubis and vertebral column is opposed by muscles originating from the ventral ischium (m. puboischiofemoralis externus (ischial portion), m. adductor femoris, and the ischial portions of m. flexor tibialis internus and m. flexor tibialis externus). The pubic portion of m. puboischiofemoralis externus, m. ambiens, and m. pubotibialis that arise from the ventral pubis have muscles from the ilium and posterior vertebral column as antagonists (m. flexor tibialis internus and m. flexor tibialis externus, m. iliofibularis,

m. iliotibialis, m. iliofemoralis, m. puboischiofemoralis internus (ischial portion)). Musculus ambiens and m. pubotibialis have m. iliofibularis as antagonist. Musculus femorotibialis and m. extensor digitorum longus arise mostly dorsally from the femur. Musculus gastrocnemius externus, m. gastrocnemius internus, and m. flexor digitorum longus arise ventrally from the femur. Musculus gastrocnemius externus and m. gastrocnemius internus, and flexor digitorum longus (flexion of digits) seem to oppose m. extensor digitorum longus (extension of digits) and m. femorotibialis (Table 3).

Muscle physiology and FESA

Muscle forces and FESA

Humerus

The compressive stress distribution and the muscle forces were computed for loadcase downstroke and upstroke of the humerus FE model. In initial FESA runs, the dorsal tuberosity of the humerus was left unloaded. Augmenting the FESA with the muscle wrapping of m. latissimus dorsi and m. subcoracoscapularis around the dorsal tuberosity revealed by LOA observations aided in loading this process with compressive stress. In addition, extensors and flexors that wrap around the anterior and posterior distal curved expansions (ectepicondylar and entepicondylar processes) of the humerus allowed to load them by compressive stress. Muscles that wrap around bone impose compressive stress onto it. Contrastingly, muscles that do not wrap around bone impose solely localized tensile loads onto the bone.

In the FESA results for the humerus (Figure 7 c, d), red, orange, and yellow correspond with low compressive stress (0 to -3,6 MPa). The dorsal tuberosity of the humerus, as well as large parts of its distal expansions, are loaded by low compressive stress. This corresponds well with the observation that the distal humerus is mostly composed of spongy bone that is covered only by a thin layer of cortical bone (compare to Krahl, 2020). The green colour spectrum correlates with moderate compressive stress (-3,6 to -7,2 MPa). Large areas of the cortical and spongy bone, especially in the region of the humerus shaft, but also in smaller regions of the distal expansions are compressed moderately (Figure 7 c, d). Turquoise to blue colours conform to high compressive stress (-7,2 to -10,8 MPa). High compressive stress partially corresponds to the outermost cortical layer. Especially the proximal region of the head and the proximal shaft are loaded by high compressive stress (Figure 7 c, d).

On the distal articulation surface of the humerus, high stress peaks occur very narrowly localized (Figure 7 c). These are artifacts which are due to the application of the counterforce. The counterforce was applied scattered over the large distal articulation surface, instead of applying it to one point, to receive a more realistic force induction. Nevertheless, this is a trade off between realistic conditions and technical software possibilities.

During the downstroke, m. pectoralis is the muscle that develops the highest muscle force (9600 N) among the muscles that span the glenoid. Surprisingly, during the upstroke, m. pectoralis still develops a higher force (5267 N) than either one of the main humerus elevators, i.e., m. latissimus dorsi and m. subcoracoscapularis. Nonetheless, both develop high muscle forces, m. subcoracoscapularis (4422 N) and m. latissimus dorsi (3918 N), to sustain the upstroke together. Generally, it becomes apparent, that greater muscle forces are produced by retractors and depressors of the humerus than by its elevators and protractors. Furthermore, extensors and flexors develop partially extremely high muscle forces, with m. flexor carpi radialis producing 8460 N during the downstroke and m. extensor digitorum communis producing 6000 N during the upstroke (Table 4).

Femur

For loadcase downstroke and upstroke of the femur FE model, the compressive stress distribution and the muscle forces were computed. In initial FESA runs of the femur, we were unable to load the dorsal trochanter and the distal epiphyses of the femur with compressive stress because the muscles would simply pull away from their origin. Thereby only localized tensile loads were observable in FESAs. Then we again introduced the LOA observations on muscle wrapping, with m. iliofemoralis and m. puboischiofemoralis internus wrapping around the dorsal trochanter and the extensor and flexors wrapping around the distally much expanded femoral epicondyles, and the respective structures were loaded by compressive stress.

The colour coding of the compressive stress distribution in the plesiosaur femur (Figure 7 c, d) is the same as for the humerus (see above). Low compressive stress correlates mostly with the medullary region in the mid to distal femur and the distal expansions of the femur. Moderate compressive stress occurs mostly in regions where cortical bone is found, especially on the outer femur shaft. The high compressive stress values correspond mostly with areas of the femoral head and part of the cortical bone of the proximal shaft (Figure 7 g, h). Like in the FESA of the humerus, localized compressive stress peaks on the distal articulation surface of the plesiosaur femur derive from the selective application of the counterforce in several points scattered across the articulation surface (see above) (Figure 7 g).

The muscle forces of the many two-joint muscles (m. pubotibialis, m. puboischiotibialis, m. flexor tibialis externus, m. flexor tibialis internus, m. ambiens, m. iliotibialis, m. iliofibularis) in the plesiosaur hindflipper cannot be determined because they influence the femur only indirectly by adding to the counterforce. During the downstroke, m. puboischiofemoralis externus produces the highest muscle force (7878 N). During the upstroke, m. puboischiofemoralis internus produces up to 7611 N. Extensor and flexor muscle forces are considerably lower in the femur than in the foreflipper. M. gastrocnemius, a flexor, develops a total force of up to 1176 N (Table 5).

Changes in muscle length

Muscles that are dorsal to the glenoid and acetabulum extend during the downstroke and contract during the upstroke. Muscles that originate ventrally to glenoid and acetabulum contract when the humerus and femur are depressed during the downstroke and are extended during the upstroke when the humerus and femur are elevated.

Total muscle length changes of the foreflipper vary between 0% and 70,87%. Three muscle (or portions thereof) (m. deltoideus clavicularis, m. triceps brachii (anterior and posterior portion) show no length change, i.e., the length changes were immeasurable with the technique employed here, meaning they are smaller than 1,7 cm (breadth of the terminal strips). Musculus coracobrachialis brevis (posterior portion) shows very little muscle shortening (3,88%). Otherwise, total muscle length changes cover the whole physiological spectrum, from around 9% in the posterior portion of m. subcoracoscapularis to 37% for the anterior portion of m. latissimus dorsi. The only muscle that stands out is ds with a total length change of over 70%. This is clearly not physiological. So a screw eye pin was alternatively screwed into the origin area of the m. deltoideus scapularis that is on the ventral to ventrolateral scapula anterior to the glenoid. The total muscle length change was measured again in all three flipper positions and ranged now within the measuring error, i.e., it ranged well within physiological boundaries (Table 1).

Total muscle length change for the hindflipper ranges from 0% to 35,8%. Musculus caudifemoralis brevis (ilium portion) and m. pubotibialis lack any length change due to methodical reasons (see above). Further, m. caudifemoralis brevis which originates from the vertebral column shows little total muscle length change at 5,2% while the muscle with the largest change (35,82%) in total muscle length is the portion of the m. puboischiofemoralis internus originating at the vertebral column (Table 1).

Looking at agonistic and antagonistic muscles, the total length changes of m. pectoralis and m. latissimus dorsi, the two muscles that mainly power down- and upstroke of the foreflipper, are fairly similar: the anterior portion of m. latissimus dorsi (36,96%) and m. pectoralis posterior portion (35,65%) and posterior m. latissimus dorsi portion (21,92%) and m. pectoralis anterior portion (18,75%). Total muscle length changes of agonists and antagonists were expected to be similar due to their opposing functions. Instead it was found that those muscles that show comparable total muscle length changes are rather determined by their geometric arrangement in relation to the glenoid or acetabulum. This means, that a muscle that originates from e.g. the posteroventral ischium (e.g. m. puboischiofemoralis externus (23,55%)) shows a rather similar shortening as one that originates from the anterodorsal pubis (m. puboischiofemoralis internus (21,04%)).

Discussion

Myology

As noted earlier, the muscle reconstructions on which this study is based on were obtained by evaluating comparative anatomical data (i.e., with the EPB) (Krahl, 2020). These biologically derived muscle reconstructions are counterchecked on whether they also meet the mechanical criteria to which muscles are subjected. Mostly we find that the reconstructed muscles are in accordance with the mechanical criteria, too. Although some changes of the plesiosaur fore- and hindflipper muscle reconstructions were made due to mechanical reasons (m. biceps brachii, m. deltoideus scapularis, m. gastrocnemius internus), i.e., in terms of receiving a more homogenous compressive stress distribution in FESA of the humerus and femur. We found mechanical evidence of support for some reconstructions made by Krahl (2020) which were rather weakly supported by the EPB (i.e., m. subcoracoscapularis from the coracoid, m. coracobrachialis brevis, m. coracobrachialis longus, m. ambiens, m. iliofemoralis, m. puboischiofemoralis).

One muscle, m. scapulohumeralis anterior was reconstructed additionally to Krahl (2020), as it could aid in humerus rotation. Convergently to Cheloniidae (Krahl et al., 2019), muscles were found that wrap around the humerus as well as the femur in plesiosaurs. The area of origin of m. scapulohumeralis anterior is situated on the anterior scapular blade. In comparison to the reconstruction by Araújo & Correia (2015), it is not as much ventral and more laterally situated. Robinson (1975) and Watson (1924) reconstructed its attachment surface on the medial and ventral scapula which is not supported by the EPB (Jenkins & Goslow, 1983; Russell & Bauer, 2008). Contrastingly, Carpenter et al. (2010) reconstructed a large origin area of m. scapulohumeralis anterior on the lateral scapula. Instead, we reconstructed a large m. deltoideus scapularis in roughly the same area which is better substantiated by the EPB (Walker, 1973; Meers, 2003; Russell & Bauer, 2008; Suzuki & Hayashi, 2010). The results presented here disagree with Tarlo (1958) in that the origin of m. scapulohumeralis anterior is on the anteroventral scapula because this is not supported by extant Sauropsida (Walker, 1973; Meers, 2003; Russell & Bauer, 2008; Suzuki & Hayashi, 2010). The sketches of the muscle reconstructions by Lingham-Soliar (2000) are solely schematic. It is impossible to determine exact muscle attachments from these drawings. Yet, judging by the geometrical arrangement, his muscle reconstructions resemble our results. M. scapulohumeralis anterior occurs exclusively in lepidosaurs and neither in turtles nor in crocodilians (Walker, 1973; Meers, 2003; Russell & Bauer, 2008; Suzuki & Hayashi, 2010). It inserts posterodorsally into the humerus in lepidosaurs; therefore, according to the EPB this pattern was transferred to the plesiosaur in this study. None of the previous authors who have reconstructed this muscle, reconstructed its insertion in this place. They either placed it at the anterodorsal humerus (Watson, 1924; Tarlo, 1958; Robinson, 1975) or at the dorsal humerus (Lingham-Soliar, 2000; Carpenter et al., 2010).

M. scapulohumeralis anterior is reconstructed in agreement with Tarlo (1958) and Watson (1924) to potentially protract the humerus subordinately and to rotate it (Watson, 1924; Tarlo, 1958). Watson (1924) and Tarlo (1958) disagree on how protraction and rotation took place. Whereas Watson (1924) proposed the muscle to rotate the humerus anteriorly upwards, Tarlo (1958) infers the opposite. Whereas Tarlo (1958) and Robinson (1975), and the current study agree on the direction of humerus rotation, Robinson (1975) additionally describes sha as a depressor, which contradicts the results of this study. A possible minor elevational function was not described by any previous author.

Muscle physiology

Total muscle length changes

Total muscle length changes were calculated for glenoid and acetabulum spanning muscles and tested whether they lie within physiological boundaries. The total muscle length change of m. deltoideus scapularis, if it would have originated from the lateral scapula, is not physiological and would not allow the muscle to produce much power (compare Biewener &

Roberts, 2000) (Table 1; Figure 6 a). This could indicate, that the muscle reconstruction of m. deltoideus scapularis on the scapula blade by Krahl (2020) is wrong, despite being well supported by the EPB, and that its origin could have been restricted to the ventral side of scapula. An origin of m. deltoideus scapularis on the ventral to ventrolateral scapula anterior to the glenoid would result in a length change that is within the physiological limits (Table 1). Further, a muscle length change within the measuring error, i.e., a small one, would actually account better for the often non-parallel and rather complex architecture of the deltoid muscle (s. e.g., Krahl et al., 2019; Walker, 1973; Meers, 2003; Russell & Bauer, 2008). A reduction of the m. deltoideus scapularis from the scapular blade would mean that no locomotory muscles attach to the lateral scapular blade in plesiosaurs ~~anymore.~~ Solely muscle attachments that suspend the shoulder girdle remain on the scapular blade. Besides aquatic adaptation (Krahl et al., 2019), this could be another explanation for why the dorsal scapular projection is so much smaller than in extant Sauropsida (compare to Walker, 1973; Meers, 2003; Russell & Bauer, 2008; Suzuki & Hayashi, 2010) and potential functional analogues (compare to Walker, 1973; English, 1977; Schreiweis, 1982; Louw, 1992; Cooper et al., 2007). Similarly, a relocation or reduction of muscles originating from the ilium (e.g., m. iliofemoralis), could free or mostly free the ilium of locomotory musculature and therefore allow its reduction.

For several muscles (e.g., m. deltoideus clavicularis, the two m. triceps brachii, m. coracobrachialis brevis (posterior portion); m. caudifemoralis brevis (ilium), m. pubotibialis), nearly isometrical conditions were determined for elevation and depression of plesiosaur humerus and femur. If one would additionally consider protraction and retraction and long axis rotation of the humerus, muscle length changes would provide different results in all of these muscles. Possibly, these almost isometrical muscles had a complex muscle architecture (see Biewener & Roberts, 2000 for a review). Additionally, it is possible that m. triceps brachii and m. pubotibialis had long tendons (i.e., a large non-contractive component. Another possibility is that those muscles that lack length changes were actually reduced in plesiosaurs. Some clues might be given by the EPB: M. triceps brachii is much reduced or entirely reduced in Chelonioidea, depending on the species. The coracobrachialis brevis is markedly reduced in size in Testudines (Walker, 1973). Possibly, the m. caudifemoralis brevis origin from the ilium was reduced in plesiosaurs and that m. caudifemoralis brevis arose only from the vertebral column. Musculus pubotibialis is absent in crocodilians (Otero, Gallina & Herrera, 2010; Suzuki et al., 2011).

Muscle length changes of agonistic and antagonistic muscles of the pelvic and pectoral girdle do not correspond well. On the one hand, this might be due to differences in the morphology and geometry of the pectoral and pelvic girdle. On the other hand, the results could also change if flipper protraction and retraction were taken into account. Further, muscle architecture and tendon length were not and most probably cannot be inferred for extinct tetrapods.

Muscle forces

Humerus

On average, forces of muscles generated during the downstroke, i.e., by the humeral and femoral depressors and retractors, appear to have higher forces than muscles involved in the upstroke (Table 4; Tab 5). This could mean that in plesiosaurs the fore- and hindflipper downstroke was more efficient than the upstroke. Similarly, the foreflipper downstroke in Cheloniidae is more powerful than the upstroke (Davenport, Munks & Oxford, 1984; Krahl et al., 2019). However, this difference in efficiency is not found in all underwater fliers because it is not found in, e.g., penguins in which the foreflipper downstroke is as efficient as the upstroke (Clark & Bemis, 1979).

The way they were reconstructed here, the m. scapulohumeralis anterior and posterior appear to be solely humeral rotators because they operate with considerably high muscle forces during the downstroke (Table 4). This way, their elevational function is minor. This is surprising because in extant Lepidosauria both muscles are rather small (Jenkins & Goslow, 1983; Russell & Bauer, 2008). Either this implies that their origin and insertion areas were enlarged in Krahl (2020) or that m. scapulohumeralis anterior and posterior muscle forces would need testing with further FESA runs. These would show whether one can receive a similarly homogenous compressive stress distribution by reallocating a large portion of the muscle force to muscles with a similar function and LOA, e.g., m. latissimus dorsi, m. subcoracoscapularis, etc. LOAs of m. scapulohumeralis anterior and m. scapulohumeralis posterior which would wrap unusually around the dorsal tuberosity in posterior to anterior direction seem to underpin the hypothetical reallocation of muscle force to another muscle as aforementioned.

A surprising result is that m. pectoralis is the muscle that develops the highest muscle force during the foreflipper upstroke (Table 4), too. Although in total humeral elevators and protractors should be presumed to produce a higher power output, otherwise foreflipper elevation and protraction become impossible. Furthermore, the pectoral girdle is suspended from the vertebral column, the rib cage, and the gastralia by muscles and tendons (e.g. (Avery & Tanner, 1964; Walker, 1973). Recent studies have shown that a swinging pectoral and pelvic girdle can contribute substantially to locomotion in extant Otariinae, Testudines, and crocodylians (Walker, 1971a; Baier & Gatesy, 2013; Mayerl, Brainerd & Blob, 2016; Schmidt, Mehlhorn & Fischer, 2016). This indicates, that the importance of the contribution to locomotion of pectoral and pelvic girdle swinging in Tetrapoda is not only underestimated in extant taxa but surely in extinct taxa, too. An actively swinging pectoral and pelvic girdle could contribute to the range of motion of the plesiosaur fore- and hindflippers and to the total force with which the flippers are beaten. Especially in the plesiosaur shoulder region, where there is no bony or cartilaginous connection to the trunk (as opposed to the pelvic region), a strong shoulder musculature and ligaments connecting the pectoral girdle with the vertebral column, the ribs, and the gastralia would be necessary.

On the dorsal foreflipper m. extensor carpi ulnaris develops rather low muscle forces (1000 N) in comparison to m. extensor digitorum communis (6000 N). Musculus flexor carpi radialis and m. flexor digitorum longus are topologically comparably arranged to extensor carpi ulnaris and m. extensor digitorum communis but on the ventral side of the foreflipper.

Contrastingly, m. flexor carpi radialis and m. flexor digitorum longus develop considerably lower muscle forces (both 1500 N) (Table 4). However, the extensor and flexor forces were only calculated based on their contribution to physiological loading of the femoral epicondyles. Extending the model by the digits could help to define them more precisely.

Femur

If one compares the muscle forces of the extensors and flexors of the plesiosaur humerus and femur, it becomes apparent that those of the femur (Table 5) are generally lower than those of the humerus (Table 4). This may be due to the fact that in the plesiosaur hindflipper, there are considerably more two-joint muscles and fewer as well as less independently operating extensors and flexors than in the foreflipper. The two-joint muscles aid in femur protraction/retraction, elevation/depression, and in knee flexion in extant Sauropsida (Snyder, 1954; Walker, 1973; Otero, Gallina & Herrera, 2010; Anzai et al., 2014), too. As the plesiosaur knee was immobile, these muscles were interpreted by Krahl (2020) to be part of the flipper long axis twisting mechanism additionally to their functions as depressors/elevators and protractors/retractors. Therefore, it is possible that the numerous two-joint muscles of the plesiosaur hindflipper partially aided in functions that were served by the much more differentiated extensors and flexors in the foreflipper (Krahl, 2020). Muscle forces of the two-joint muscles could not be determined in this study because they only indirectly influence FESA by adding to the counterforce imposed by the tibia and fibula. Therefore, it can be expected that the only extensor and the two flexors of the hindflipper should have in total lower muscle forces than the numerous extensors and flexors of the foreflipper. Finally, femur and humerus differ morphologically by the distal expansion, and possibly the hindflipper contributed less to propulsion than the foreflipper, as proposed by Lingham-Soliar (2000) and Liu et al. (2015).

Comparison to Cheloniidae humerus

There are some similarities in muscle forces of certain muscles in *Cryptoclidus eurymerus* (IGPB R 324) and in Cheloniidae: m. pectoralis develops the highest force of all muscles that insert proximally into the humerus (Krahl et al., 2019). Furthermore, of the main humeral elevators, m. subcoracoscapularis generates higher forces than m. latissimus dorsi in both taxa (Krahl et al., 2019). Musculus coracobrachialis brevis develops lower force in sea turtles (Krahl et al., 2019) than in plesiosaurs. Contrastingly, m. coracobrachialis longus develops higher forces in sea turtles (Krahl et al., 2019) than in plesiosaurs. While m. deltoideus scapularis and m. deltoideus clavicularis contribute in markedly different ways to propulsion in Cheloniidae (Krahl et al., 2019), they operate with broadly similar forces in plesiosaurs.

Another difference between the forces of humerus muscles of cheloniids (Krahl et al., 2019) and plesiosaurs is that in the former they vary by an order of magnitude unlike in the latter in which they do not necessarily differ much. These results support a hydrodynamic study of *Cryptoclidus eurymerus* (IGPB R 324) that finds flipper twisting to be crucial for underwater flight in plesiosaurs (Witzel, Krahl & Sander, 2015; Witzel, 2020). Furthermore, these findings corroborate the myological flipper twisting mechanism proposed by (Krahl et al., 2019). Generally, higher muscle forces in plesiosaurs could be due to scaling effects.

The muscle bellies that produce these enormous muscle forces (up to 9600 N) in the shoulder girdle were large and took much space. Therefore, it is indeed problematic that extensors and flexors proved to have produced similarly large forces because their potential origin surfaces are much smaller than for the glenoid spanning muscles. Different solutions to this paradox may exist. M. flexor digitorum longus, for instance, has a second head arising from the carpus in Sauropsida (Walker, 1973; Meers, 2003; Russell & Bauer, 2008), so it could have been able to develop substantially higher force, than just by the humeral muscle belly. Further, possibly these muscles have a complex architecture that saves space in comparison to the musculature originating from the pectoral girdle. Long tendinous structures could have been a mechanism to conserve energy during cruising (Roberts et al., 1997; Biewener & Roberts, 2000).

Dolphins have a relatively well ossified flipper skeleton, although there are basically no individual muscles identifiable anymore. They merely have layers of parallel fibred connective tissue covering the flipper bones (see Cooper et al., 2007, Figure 4, p. 1128). This means in reverse that the hydrodynamic forces plus the „muscle“ force these layers of connective tissue can exert are in total enough to induce ossification of the flipper bones. Similar aponeurotic layerings, maybe also directed in the main directions of flipper twisting could account for a considerable part of the muscle forces calculated with FESA. Also, the connective tissue covering the broad space of the non-functional elbow joint, carpus, and manus could passively also conserve energy and thus passively compensate for some of the forces computed.

Conclusions

The highly aquatically adapted locomotor apparatus of plesiosaurs experienced little change throughout 135 Ma of plesiosaur evolution. The question of whether plesiosaurs rowed, flew underwater, or employed a combination of both has not been fully answered yet. Here we present a computer model which is in agreement with underwater flight in plesiosaurs based on comparative anatomical and muscle physiological data in accordance with mechanical principles. For this purpose, a foreflipper and hindflipper cast of IGPB R 324 were mounted on a wooden framework. With the help of screw eye pins, electrical terminal strips, and threads humerus and femur muscle LOA were recreated. Three positions representing maximum dorsal and ventral fore- and hindflipper excursion and a neutral position were fixed with ropes. For each muscle that spans glenoid and acetabulum muscle length was measured in all three positions. Then total muscle length changes over a flipper beat cycle were calculated for all muscles. A *Cryptoclidus* humerus and femur FE model were built from micro-CT scans of IGPB R 324. Then, FESA was conducted for load case downstroke and upstroke for both long bones. Muscle insertion angles were obtained from LOA recreation. Muscle forces were stochastically determined in iterative steps.

We demonstrate that by aiming at a homogenous compressive stress distribution in the humerus and femur of *Cryptoclidus* (IGPB R 324), it is possible to test muscle reconstructions and their associated LOA with FESA. Muscle reconstructions by Krahl (2020) were found to be largely corroborated, but they were also amended and corrected due to FESA. As in Cheloniidae, muscles wrapping around bony processes, i.e., the dorsal tuberosity of the plesiosaur humerus and dorsal trochanter of the plesiosaur femur, as well as their epicondyles, proved to be necessary to load the aforementioned structures. Further, measuring the total length changes of all muscles that insert into, originate from, and span humerus and femur of a plesiosaur showed that a m. deltoideus scapularis origin from the lateral scapula is unphysiological. This infers a reduction of this muscle from this part of its origin site which is well supported across Sauropsida (Walker, 1973; Meers, 2003; Russell & Bauer, 2008). Muscle forces show some correlation with cheloniid humerus musculature but also differences which underlines that underwater flight in both lineages was achieved in convergent ways. High extensor and flexor forces in plesiosaurs corroborate the hypothesis that flipper long axis twisting was essential for plesiosaur underwater flight.

Acknowledgements

We are grateful to Aart Walen (Creatures and Features), Arnhem, The Netherlands, for kindly providing a cast of the pectoral and pelvic girdle and foreflipper and hindflipper of IGPB R 324 that was crucial to this study. The authors greatly appreciate the help of L. Baumeister of the Biomechanics Research Group, Chair of Product Development, Faculty of Mechanical Engineering, Ruhr-University Bochum, Germany, with FE models of the femur. The authors thank Tanja Wintrich (Bonn) for producing the micro-CT scans of the humerus and femur of IGPB R 324. This study was funded by Deutsche Forschungsgemeinschaft (DFG) grant WI1389/8-1.

References

Alexander RM, Vernon A. 1975. The dimensions of knee and ankle muscles and the forces they exert. *Journal of Human Movement Studies* **1**:115–123.

Allen V, Elsey RM, Jones N, Wright J, Hutchinson JR. 2010. Functional specialization and ontogenetic scaling of limb anatomy in *Alligator mississippiensis*. *Journal of Anatomy* **216 (4)**:423–445.

Anapol F, Barry K. 1996. Fibre architecture of the extensors of the hindlimb in semiterrestrial and arboreal guenons. *American Journal of Physical Anthropology* **99**:429-447.a.

Andrews CW. 1910. A Descriptive Catalogue of the Marine Reptiles of the Oxford Clay, Part I. London, UK: British Museum (Natural History).

Anzai W, Omura A, Diaz AC, Kawata M, Endo H. 2014. Functional morphology and comparative anatomy of appendicular musculature in Cuban *Anolis* lizards with different locomotor habits. *Zoological Science* **31 (7)**:454–463.

Araújo R, Correia F. 2015. Soft-tissue anatomy of the plesiosaur pectoral girdle inferred from basal Eosauropterygia taxa and the extant phylogenetic bracket. *Palaeontologia Electronica* **18 (1)**:1–32.

Araújo R, Polcyn MJ, Schulp AS, Mateus O, Jacobs LL, Gonçalves AO, Morais M-L. 2015. A new elasmosaurid from the early Maastrichtian of Angola and the implications of girdle morphology on swimming style in plesiosaurs. *Netherlands Journal of Geosciences - Geologie en Mijnbouw* **94 (1)**:109–120.

Avery, F D, Tanner WW. 1964. The osteology and myology of the head and thorax regions of the obesus group of the genus *Sauromalus dumeril* (Iguanidae). *Brigham Young University Science Bulletin, Biological Series* **5 (3)**:1–30.

Azizi E, Brainerd EL, Roberts TJ. 2008. Variable gearing in pennate muscles. *Proceedings of the National Academy of Sciences of the United States of America* **105 (5)**:1745–1750.

Baier DB, Gatesy SM. 2013. Three-dimensional skeletal kinematics of the shoulder girdle and forelimb in walking *Alligator*. *Journal of Anatomy* **223 (5)**:462–473.

Bardet N. 1994. Extinction events among Mesozoic marine reptiles. *Historical Biology* **7 (4)**:313–324.

Bardet N, Falconnet J, Fischer V, Houssaye A, Jouve S, Pereda Suberbiola X, Pérez-García A, Rage J-C, Vincent P. 2014. Mesozoic marine reptile palaeobiogeography in response to drifting plates. *Gondwana Research* **26 (3–4):869–887.**

Baudinette RV, Gill P. 1985. The energetics of 'flying' and 'paddling' in water: Locomotion in penguins and ducks. *Journal of Comparative Physiology B* **155 (3)**:373–380.

Biewener AA, Corning WR, Tobalske BW. 1998. In vivo pectoralis muscle force-length behavior during level flight in pigeons (*Columba livia*). *Journal of Experimental Biology* **201 (24)**:3293–3307.

Biewener AA, Dial KP. 1995. In vivo strain in the humerus of pigeons (*Cloumba livia*) during flight. *Journal of Morphology* **225**:61–65.

Biewener AA, Konieczynski DD, Baudinette RV. 1998. In vivo muscle force-length behavior during steady-speed hopping in tammar wallabies. *Journal of Experimental Biology* **201 (11)**:1681–1694.

Biewener AA, Roberts TJ. 2000. Muscle and tendon contributions to force, work, and elastic energy savings: A comparative perspective. *Exercise and Sport Sciences Reviews* **28 (3)**:99–107.

Blob RW, Biewener AA. 1999. In vivo locomotor strain in the hindlimb bones of *Alligator mississpiensis* and *Iguana iguana*: Implications for the evolution of limb bone safety factor and non-sprawling limb posture. *Journal of Experimental Biology* **202**:1023–1046.

Bryant HN, Russel AP. 1992. The role of phylogenetic analysis in the inference of unpreserved attributes of extinct taxa. *Philosophical Transactions of the Royal Society London B* **337**:405–418.

Burkholder TJ, Fingado B, Bron S, Lieber R. 1994. Relationship between muscle fiber types and sizes and muscle architectural properties in the mouse hindlimb. *Journal of Morphology* **221**:177–199.

Butcher MT, Blob RW. 2008. Mechanics of limb bone loading during terrestrial locomotion in river cooter turtles (*Pseudemys concinna*). *Journal of Experimental Biology* **211 (8)**:1187–1202.

Butcher MT, Espinoza NR, Cirilo SR, Blob RW. 2008. In vivo strains in the femur of river cooter turtles (*Pseudemys concinna*) during terrestrial locomotion: Tests of force-platform models of loading mechanics. *Journal of Experimental Biology* **211 (15)**:2397–2407.

Caldwell MW. 1997. Limb osteology and ossification patterns in *Cryptoclidus* (Reptilia: Plesiosauroidea) with a review of Sauropterygian limbs. *Journal of Vertebrate Paleontology* **17 (2)**:295–307.

Carpenter K, Sanders F, Reed B, Reed J, Larson P. 2010. Plesiosaur swimming as interpreted from skeletal analysis and experimental results. *Transactions of the Kansas Academy of Science* **113 (1/2)**:1–34.

Carrano MT. 1998. Locomotion in non-avian dinosaurs: Integrating data from hindlimb kinematics, in vivo strains, and bone morphology. *Paleobiology* **24 (04)**:450–469.

Carter DR, Orr TE, Fyhrie DP. 1989. Relationships between loading history and femoral cancellous bone architecture. *Journal of Biomechanics* **22 (3)**:231–244.

Clark BD, Bemis W. 1979. Kinematics of swimming of penguins at the Detroit Zoo. *Journal of Zoology* **188 (3)**:411–428.

Cooper LN, Dawson SD, Reidenberg JS, Berta A. 2007. Neuromuscular anatomy and evolution of the cetacean forelimb. *The Anatomical Record* **290 (9)**:1121–1137.

Curtis N, Witzel U, Fitton L, O'Higgins P, Fagan MJ. 2011. The mechanical significance of the temporal fasciae in *Macaca fascicularis*: An investigation using finite element analysis. *The Anatomical Record* **294 (7)**:1178–1190.

Davenport J, Munks SA, Oxford PJ. 1984. A comparison of the swimming of marine and freshwater turtles. *Proceedings of the Royal Society B: Biological Sciences* **220 (1221)**:447–475.

Elliott KH, Ricklefs RE, Gaston AJ, Hatch SA, Speakman JR, Davoren GK. 2013. High flight costs, but low dive costs, in auks support the biomechanical hypothesis for flightlessness in penguins. *Proceedings of the National Academy of Sciences of the United States of America* **110 (23)**:9380–9384.

English AWM. 1977. Structural correlates of forelimb function in fur seals and sea lions. *Journal of Morphology* **151 (3)**:325–352.

Feldkamp SD. 1987. Foreflipper propulsion in the California sea lion, *Zalophus californianus*. *Journal of Zoology* **212**:43–57.

Felsenthal N, Zelzer E. 2017. Mechanical regulation of musculoskeletal system development. *Development* **144 (23)**:4271–4283.

Fish FE. 1996. Transitions from drag-based to lift-based propulsion in mammalian swimming. *American Zoologist* **36 (6)**:628–641.

Fish FE. 2002. Balancing requirements for stability and maneuverability in cetaceans. *Integrative and Comparative Biology* **42**:85–93.

Fish FE. 2004. Structure and mechanics of nonpiscine control surfaces. *IEEE Journal of Oceanic Engineering* **29 (3)**:605–621.

Fish FE, Battle JM. 1995. Hydrodynamic design of the humpback whale flipper. *Journal of Morphology* **225 (1)**:51–60.

Frey E, Riess J. 1982. Considerations concerning plesiosaur locomotion. *Neues Jahrbuch für Geologie und Paläontologie, Abhandlungen* **164**:193–194.

Gans C. 1982. Fibre architecture and muscle function. *Exercise and Sport Science Reviews* **10 (1)**:160–207.

Godfrey SJ. 1984. Plesiosaur subaqueous locomotion: a reappraisal. *Neues Jahrbuch für Geologie und Palaontologie Monatshefte*:661–672.

Großmann F. 2006. Taxonomy, phylogeny and palaeoecology of the plesiosauroids (Sauropterygia, Reptilia) from the Posidonia shale (Toarcian, Lower Jurassic) of Holzmaden, south west Germany. Dissertation, Eberhard-Karls-Universität.

Huq E, Wall CE, Taylor AB. 2015. Epaxial muscle fiber architecture favors enhanced excursion and power in the leaper *Galago senegalensis*. *Journal of Anatomy*.

Jenkins FA, Goslow GE. 1983. The functional anatomy of the shoulder of the savannah monitor lizard (*Varanus exanthematicus*). *Journal of Morphology* **175**:195–216.

Klenner S, Witzel U, Paris F, Distler C. 2015. Structure and function of the septum nasi and the underlying tension chord in crocodylians. *Journal of Anatomy* **228 (1)**:113–124.

Krahl A. 2020. Underwater flight in sea turtles and plesiosaurs ─ Dissection, muscle reconstructions, analog models, and finite element structure analyses inform on flipper twisting and muscle forces in plesiosaurs. PhD-dissertation, Mathematisch-Naturwissenschaftliche Fakultät der Rheinischen Friedrich-Wilhelms-Universität Bonn, Bonn. p.311. https://nbn-resolving.org/urn:nbn:de:hbz:5-59143.

Krahl A, Lipphaus A, Witzel U, Sander PM, Maffucci F, Hochscheid S. 2019. Humerus osteology, myology, and finite element structure analysis of Cheloniidae. *The Anatomical Record* **303 (8)**: 2177-2191. https://doi.org/10.1002/ar.24311.

Kummer B. 2005. *Biomechanik*. Köln: Deutscher Ärzte Verlag.

Lieberman DE, Polk JD, Demes B. 2004. Predicting long bone loading from cross-sectional geometry. *American Journal of Physical Anthropology* **123 (2)**:156–171.

Lingham-Soliar T. 2000. Plesiosaur locomotion: Is the four-wing problem real or merely an atheoretical exercise? *Neues Jahrbuch für Geologie und Paläontologie, Abhandlungen* **217 (1)**:45–87.

Lipphaus A, Witzel U. 2018. Biomechanical study of the development of long bones: Finite element structure synthesis of the human second proximal phalanx under growth conditions. *The Anatomical Record*.

Liu S, Smith AS, Gu Y, Tan J, Liu CK, Turk G. 2015. Computer simulations imply forelimb-dominated underwater flight in plesiosaurs. *PLoS Computational Biology* **11 (12)**:e1004605.

Louw GJ. 1992. Functional anatomy of the penguin flipper. *Journal of the South African Veterinary Association* **63 (3)**:113–120.

Lutz F, Mastel R, Runge M, Stief F, Schmidt A, Meurer A, Witte H. 2016. Calculation of muscle forces during normal gait under consideration of femoral bending moments. *Medical Engineering & Physics* **38 (9)**:1008–1015.

Main RP, Biewener AA. 2004. Ontogenetic patterns of limb loading, in vivo bone strains and growth in the goat radius. *The Journal of Experimental Biology* **207 (15)**:2577–2588.

Main RP, Biewener AA. 2007. Skeletal strain patterns and growth in the emu hindlimb during ontogeny. *The Journal of Experimental Biology* **210 (15)**:2676–2690.

Mayerl CJ, Brainerd EL, Blob RW. 2016. Pelvic girdle mobility of cryptodire and pleurodire turtles during walking and swimming. *The Journal of Experimental Biology* **219 (Pt 17)**:2650–2658.

McCabe K, Henderson K, Pantinople J, Richards HL, Milne N. 2017. Curvature reduces bending strains in the quokka femur. *PeerJ* **5**:e3100.

Meers MB. 2003. Crocodylian forelimb musculature and its relevance to Archosauria. *The Anatomical Record* **274 (2)**:891–916.

Merck JW. 1997. A phylogenetic analysis of the euryapsid reptiles. *Journal of Vertebrate Paleontology* **17**:65.

Milne N. 2016. Curved bones: An adaptation to habitual loading. *Journal of Theoretical Biology* **407**:18–24.

Motani R. 2009. The evolution of marine reptiles. *Evolution: Education and Outreach* **2 (2)**:224–235.

Muscutt LE, Dyke G, Weymouth GD, Naish D, Palmer C, Ganapathisubramani B. 2017. The four-flipper swimming method of plesiosaurs enabled efficient and effective locomotion. *Proceedings of the Royal Society B: Biological Sciences)* **284 (1861)**:20170951.

Narici MV, Landoni L, Minetti AE. 1992. Assessment of human knee extensor muscles stress from in vivo physiological cross-sectional area and strength measurements. *European Journal of Applied Physiology and Occupational Physiology* **65 (5)**:438–444.

Neenan JM, Klein N, Scheyer TM. 2013. European origin of placodont marine reptiles and the evolution of crushing dentition in Placodontia. *Nature Communications* **4**:1621.

Otero A, Gallina PA, Herrera Y. 2010. Pelvic musculature and function of *Caiman latirostris*. *Herpetological Journal* **20**:173–184.

Pace CM, Blob RW, Westneat MW. 2001. Comparative kinematics of the forelimb during swimming in red-eared slider (*Trachemys scripta*) and spiny softshell (*Apalone spinifera*) turtles. *The Journal of Experimental Biology* **204**:3261–3271.

Pinshow B, Fedak MA, Schmidt-Nielsen K. 1977. Terrestrial locomotion in penguins: It costs more to waddle. *Science* **195 (4278)**:592–594.

Powell PL, Roy RR, Kanim P, Bello MA, Edgerton VR. 1984. Predictability of skeletal muscle tension from architectural determinations in guinea pig hindlimbs. *Journal of Applied Physiology* **57 (6)**:1715–1721.

Rassier DE, MacIntosh BR, Herzog W. 1999. Length dependence of active force production in skeletal muscle. *Journal of Applied Physiology* **86 (5)**:1445–1457.

Rayfield EJ. 2007. Finite element analysis and understanding the biomechanics and evolution of living and fossil organisms. *Annual Review of Earth and Planetary Sciences* **35 (1)**:541–576.

Rhodin AGJ, Ogden JA, Conlogue GJ. 1981. Chondro-osseous morphology of *Dermochelys coriacea*, a marine reptile with mammalian skeletal features. *Nature* **290**:244.

Rieppel O, Reisz RR. 1999. The origin and early evolution of turtles. *Annual Review of Ecology and Systematics* **30**:1–22.

Rivera ARV, Rivera G, Blob RW. 2013. Forelimb kinematics during swimming in the pig-nosed turtle, *Carettochelys insculpta*, compared with other turtle taxa: Rowing versus flapping, convergence versus intermediacy. *The Journal of Experimental Biology* **216 (Pt 4)**:668–680.

Rivera ARV, Wyneken J, Blob RW. 2011. Forelimb kinematics and motor patterns of swimming loggerhead sea turtles (*Caretta caretta*): Are motor patterns conserved in the evolution of new locomotor strategies? *The Journal of Experimental Biology* **214 (19)**:3314–3323.

Rivera G, Rivera ARV, Blob RW. 2011. Hydrodynamic stability of the painted turtle (*Chrysemys picta*): Effects of four-limbed rowing versus forelimb flapping in rigid-bodied tetrapods. *The Journal of Experimental Biology* **214 (Pt 7)**:1153–1162.

Roberts TJ, Marsh RL, Weyand PG, Taylor CR. 1997. Muscular force in running turkeys: The economy of minimizing work. *Science* **275 (5303)**:1113–1115.

Robinson JA. 1975. The locomotion of plesiosaurs. *Neues Jahrbuch für Geologie und Paläontologie, Abhandlungen* **149**:286–332.

Robinson JA. 1977. Intracorporal force transmission in plesiosaurs. *Neues Jahrbuch Geologie Paläontologie, Abhandlungen* **153**:86–128.

Russell AP, Bauer AM. 2008. The appendicular locomotor apparatus of *Sphenodon* and normal-limbed squamates. In: Gans C, Parsons TS, editors. *Biology of the Reptilia* Volume 21 New York: Academic Press. 1–465.

Sachs S, Hornung JJ, Kear BP. 2016. Reappraisal of Europe's most complete Early Cretaceous plesiosaurian: *Brancasaurus brancai* Wegner, 1914 from the "Wealden facies" of Germany. *PeerJ* **4**:e2813.

Sacks RD, Roy RR. 1982. Architecture of the hind limb muscles of cats: Functional significance. *Journal of Morphology* **173 (2)**:185–195.

Schmidt M, Mehlhorn M, Fischer MS. 2016. Shoulder girdle rotation, forelimb movement and the influence of carapace shape on locomotion in *Testudo hermanni* (Testudinidae). *The Journal of Experimental Biology* **219 (Pt 17)**:2693–2703.

Schreiweis DO. 1982. A comparative study of the appendicular musculature of penguins (Aves: Sphenisciformes). *Smithsonian Contributions to Zoology* **341**:1–46.

Sheffield KM, Butcher MT, Shugart SK, Gander JC, Blob RW. 2011. Locomotor loading mechanics in the hindlimbs of tegu lizards (*Tupinambis merianae*): Comparative and evolutionary implications. *The Journal of Experimental Biology* **214 (15)**:2616–2630.

Shufeldt RW. 1901. Osteology of the penguins. *Journal of Anatomy and Physiology* **35 (3)**:390–405.

Snover ML, Rhodin AGJ. 2008. Comparative ontogenetic and phylogenetic aspects of chelonian chondro-osseous growth and skeletochronology. In: Wyneken J, Godfrey MH, Bels V, eds. *Biology of Turtles.* Boca Raton, Florida, USA: CRC Press, 17–43.

Snyder RC. 1954. The anatomy and function of the pelvic girdle and hindlimb in lizard locomotion. *The American Journal of Anatomy* **95 (1)**:1–45.

Sues H-D. 1987. Postcranial skeleton of *Pistosaurus* and interrelationships of the Sauropterygia (Diapsida). *Zoological Journal of the Linnean Society* **90**:109–131.

Suzuki D, Chiba K, Tanaka Y, Hayashi S. 2011. Myology of crocodiles III: Pelvic girdle and hindlimb. *Fossils The Palaeontological Society of Japan* **90**:37–60.

Suzuki D, Hayashi S. 2010. Myology of crocodiles II: Pectoral girdle and forelimb. *Fossils The Palaeontological Society of Japan* **87**:83–102.

Sverdlova NS, Witzel U. 2010. Principles of determination and verification of muscle forces in the human musculoskeletal system: Muscle forces to minimise bending stress. *Journal of Biomechanics* **43 (3)**:387–396.

Tarlo LB. 1958. The scapula of *Pliosaurus macromerus* Phillips. *Palaeontology* **1**:193–199.

Tarsitano S, Riess J. 1982. Plesiosaur locomotion: Underwater flight versus rowing. *Neues Jahrbuch für Geologie und Paläontologie, Abhandlungen* **164**:188–192.

Taylor MA. 1989. Sea-saurians for sceptics. *Nature* **338 (6217)**:625–626.

Vincent P, Bardet N, Houssaye A, Amaghzaz M, Meslouh S. 2013. New plesiosaur specimens from the Maastrichtian phosphates of Morocco and their implications for the ecology of the latest Cretaceous marine apex predators. *Gondwana Research* **24 (2)**:796–805.

Vincent P, Bardet N, Pereda Suberbiola X, Bouya B, Amaghzaz M, Meslouh S. 2011. *Zarafasaura oceanis*, a new elasmosaurid (Reptilia: Sauropterygia) from the Maastrichtian Phosphates of Morocco and the palaeobiogeography of latest Cretaceous plesiosaurs. *Gondwana Research* **19 (4)**:1062–1073.

Walker JA, Westneat MW. 2000. Mechanical performance of aquatic rowing and flying. *Proceedings of the Royal Society of London B: Biological Sciences* **267 (1455)**:1875–1881.

Walker WF. 1971a. A structural and functional analysis of walking in the turtle, *Chrysemys picta marginata*. *Journal of Morphology* **134 (2)**:195–214.

Walker WF. 1971b. Swimming in sea turtles of the family Cheloniidae. *Copeia* **1971**:229–233.

Walker WF. 1973. The locomotor apparatus of Testudines. In: Gans C, Parsons TS, editors. *Biology of Reptilia* Volume 4. New York: Academic Press.1–100.

Watson DMS. 1924. The elasmosaurid shoulder-girdle and fore-limb. *Proceedings of the Zoological Society of London* **58**:885–917.

Williamson MR, Dial KP, Biewener AA. 2001. Pectoralis muscle performance during ascending and slow level flight in mallards (*Anas platyrhynchos*). *Journal of Experimental Biology* **204 (3)**:495–507.

Williston SW. 1914. *Water reptiles of the past and present*. Chicago, USA: University of Chicago Press.

Wintrich T, Hayashi S, Houssaye A, Nakajima Y, Sander PM. 2017. A Triassic plesiosaur skeleton and bone histology inform on evolution of a unique body plan. *Science Advances* **3 (12)**:e1701144.

Wittmer LM. 1995. The Extant Phylogenetic Bracket and the importance of reconstructing soft tissues in fossils. In: Thomason JJ, ed. *Functional Morphology in Vertebrate Paleontology.* New York: Cambridge University Press, 19–33.

Witzel, U. 2020. Funktionsmorphologische Forschung mit Hilfe biomechanischer Ansätze im Rahmen der Phylogenie und ontogenetischen Entwicklung zum Vertebraten. In: Werneburg I, Betz O, eds. *Phylogenie, Funktionsmorphologie und Bionik –Schriften zum 60. Phylogenetischen Symposium in Tübingen*. Tübingen, Germany: Scidinge Hall Verlag, 187-220.

Witzel U, Mannhardt J, Goessling R, Micheli Pd, Preuschoft H. 2011. Finite element analyses and virtual syntheses of biological structures and their application to sauropod skulls. In: Klein, N., Remes, K., Gee, C. T., & Sander, P. M., ed. *Biology of the Sauropod Dinosaurs: Understanding the Life of Giants*, 171–182.

Witzel U, Preuschoft H. 2005. Finite-element model construction for the virtual synthesis of the skulls in vertebrates: Case study of *Diplodocus*. *The Anatomical Record* **283 (2)**:391–401.

Witzel U, Krahl A, Sander PM. 2015. Hydrodynamische Untersuchung des Schimmvorgangs eines jurassischen Plesiosauriers: Bestimmung des Körperwiderstands und der Vortriebskräfte der Flossen. *ZfB-Scriptum Veröffentlichungen des Zentrums für Biodokumentation (ZfB)* **4 (58)**.

Woodward BL, Winn JP, Fish FE. 2006. Morphological specializations of baleen whales associated with hydrodynamic performance and ecological niche. *Journal of Morphology* **267 (11)**:1284–1294.

Wyneken J. 1997. Sea turtle locomotion: Mechanisms, behavior, and energetics. In: Lutz PL, Musick JA, eds. *The Biology of Sea Turtles.* Boca Raton, Florida, USA: CRC Press, 165–198.

Young VKH, Blob RW. 2015. Limb bone loading in swimming turtles: Changes in loading facilitate transitions from tubular to flipper-shaped limbs during aquatic invasions. *Biology Letters* **11 (6)**:20150110.

Young VKH, Wienands CE, Wilburn BP, Blob RW. 2017. Humeral loads during swimming and walking in turtles: Implications for morphological change during aquatic reinvasions. *The Journal of Experimental Biology* **220 (21)**:3873–3877.

Zug GR. 1971. Buoyancy, locomotion, morphology of the pelvic girdle and hindlimb, and systematics of cryptodiran turtles: University of Michigan Museum of Zoology.

Table 1(on next page)

Changes in length of *Cryptoclidus eurymerus* (IGPB R 324) humerus and femur muscles

Musculus	number coding for muscle (portion) in respective diagram	maximum ventral excursion [cm]	neutral position [cm]	maximum dorsal excursion [cm]	muscle length change (- = shortening, + = lengthening) from neutral position to maximum ventral excursion [cm]	muscle length change (- = shortening, + = lengthening) from neutral position to maximum ventral excursion [%]	muscle length change (- = shortening, + = lengthening) from neutral position to maximum dorsal excursion [cm]	muscle length change (- = shortening, + = lengthening) from neutral position to maximum dorsal excursion [%]	muscle stretching = muscle neutral position (=100%) + muscle lengthening [%]	muscle contraction = muscle neutral position (=100%) - shortening of muscle [%]	total length change of muscle [%] (= muscle stretching - muscle contraction)
m. deltoideus scapularis	1	22,2	13,6	9,8	8,6	63,24	-3,8	-7,63	163,24	92, 37	70,87
m. deltoideus scapularis corrected	2	22,6	22,6	22,6	0	0	0	0	100	100	0
m. deltoideus clavicularis	3	36,5	36,5	36,5	0	0	0	0	100	100	0
m. latissimus dorsi (anterior)	4	42,7	34,9	29,8	7,8	22,35	-5,1	-14,61	122,35	85,39	36,96
m. latissimus dorsi (in between)	5	43,9	37,6	32,6	6,3	16,76	-5	-13,3	116,76	86,7	30,06
m. latissimus dorsi (posterior)	6	52,7	47,9	42,2	4,8	10,02	-5,7	-11,9	110,02	88,1	21,92
m. subcoracoscapularis (anterior portion)	7	32,8	29,3	24,3	3,5	11,95	-5	-17,06	111,95	82,94	29,01
m. subcoracoscapularis (posterior portion)	8	36,3	33,2	33,2	3,1	9,34	0	0	109,34	100	9,34

m. scapulohumeralis anterior	9	30,9	29,5	27,4	1,4	4,75	-2,1	-7,12	104,75	92,88	11,87
m. scapulohumeralis posterior	10	24,9	22,7	19,4	2,2	9,69	-3,3	-14,54	109,69	85,46	24,23
m. coracobrachialis brevis (anterior)	11	29,3	36,7	40,5	-7,4	-20,16	3,8	10,35	110,35	79,84	30,51
m. coracobrachialis brevis (posterior)	12	43,8	43,8	45,5	0	0	1,7	3,88	103,88	100	3,88
m. coracobrachialis longus	13	43,1	52	53,9	-8,9	-17,12	1,9	3,65	103,65	82,88	20,77
m. pectoralis (anterior)	14	29,9	30,4	35,6	-0,5	-1,64	5,2	17,11	117, 11	98,36	18,75
m. pectoralis (posterior)	15	27,4	33,1	39,2	-5,7	-17,22	6,1	18,43	118,43	82,78	35,65
m. supracoracoideus	16	24,5	31,7	31,7	-7,2	-22,71	0	0	100	77,29	22,71
m. biceps brachii	17	56,7	67,8	72,4	-11,1	-16,37	4,6	6,78	106,78	83,63	23,15
m. triceps brachii (anterior)	18	36,8	36,8	36,8	0	0	0	0	100	100	0
m. triceps brachii (posterior)	19	31,2	31,2	31,2	0	0	0	0	100	100	0

Musculus	number coding for muscle (portion) in respective	maximum ventral excursion [cm]	neutral position [cm]	maximum dorsal excursion [cm]	muscle length change (- = shortening, + = lengthening)	muscle length change (- = shortening, + = lengthening) from neutral	muscle length change (- = shortening, + = lengthening) from neutral	muscle length change (- = shortening, + = lengthening) from neutral	muscle stretching = muscle neutral position (=100%) +	muscle contraction = muscle neutral position (=100%) - shortening of	total length change of muscle [%] (= muscle stretching -

	diagram				from neutral position to maximum ventral excursion [cm]	position to maximum ventral excursion [%]	position to maximum dorsal excursion [cm]	position to maximum dorsal excursion [%]	muscle lengthening [%]	muscle [%]	muscle contraction)
m. caudofemoralis longus	1	61,3	63,5	64,6	-2,2	-3,46	1,1	6,15	106,15	96,54	9,61
m. caudofemoralis brevis (ilium)	2	17,9	17,9	17,9	0	0	0	0	100	100	0
m. caudofemoralis brevis (vc)	3	37,6	36,9	33,6	0,7	1,9	-3,3	-8,94	101,9	96,7	5,2
m. flexor tibialis internus (vc)	4	63,7	58,4	52,3	5,3	9,8	-6,1	-10,45	109,8	93,9	15,9
m. flexor tibialis internus (ischium)	5	43,1	47,1	49,2	-4	-8,49	2,1	4,46	104,46	91,51	12,95
m. flexor tibialis externus (ischium)	6	42,8	47,5	49,4	-4,7	-9,89	1,9	4	104	90,11	13,89
m. flexor tibialis externus (ilium)	7	42,6	37,2	31,9	5,4	14,52	-5,3	-14,25	114,52	85,75	28,77
m. iliofibularis	8	33,1	29	25,3	4,1	14,13	-3,7	-12,76	114,13	87,24	26,89
m. ambiens	9	29,3	29,3	31,7	0	0	2,4	8,19	108,19	100	8,19
m. puboischiotibialis	10	38,3	42,3	45,8	-4	-9,46	3,5	8,27	108,27	90,54	17,73
m. pubotibialis	11	33,4	33,4	33,4	0	0	0	0	100	100	0
m. iliofemoralis	12	18,3	14,2	13,6	4,1	28,87	-0,6	-4,23	128,87	95,77	33,1
m. ischiotrochantericus	13	21,5	21,5	23,7	0	0	2,2	10,23	110,23	100	10,32
m. iliotibialis	14	40,1	26,6	26,6	7,3	27,44	0	0	127,44	100	27,44
m. adductor femoris (anterior)	15	30,4	32,8	36,2	-2,4	-7,31	3,4	6,71	106,71	92,69	14,02

m. adductor femoris (lateroposterior)	16	26,6	30	32,9	-3,4	-11,33	2,9	9,67	109,67	88,67	21
m. puboischiofemoralis internus (pubis)	17	36,8	32,3	30,3	4,5	14,85	-2	-6,19	114,85	93,81	21,04
m. puboischiofemoralis internus (ischium)	18	29,4	27,2	23,3	2,2	8,09	-3,9	-14,34	108,09	85,66	22,43
m. puboischiofemoralis internus (ilium)	19	10,4	9,5	9,5	0,9	9,47	0	0	109,47	100	9,47
m. puboischiofemoralis internus (vertebral column)	20	39,6	32,1	28,1	7,5	23,36	-4	-12,46	123,36	87,54	35,82
m. puboischiofemoralis externus (pubis)	21	39,1	42,5	45,7	-3,4	-8	3,2	7,5	107,5	92	15,5
m. puboischiofemoralis externus (ischium)	22	22,9	27,6	29,4	-4,7	-17,03	1,8	6,52	106,52	82,97	23,55

2

Table 2 (on next page)

Agonistic and antagonistic humerus muscles of *Cryptoclidus eurymerus* (IGPB R 324)

agonists	**antagonists**
anterior portion of m. latissimus dorsi (eventually m. scapulohumeralis posterior and m. scapulohumeralis anterior) (elevation, protraction)	posterior portion m. pectoralis (depression and retraction)
posterior portion of m. latissimus dorsi (elevation, retraction)	anterior portion of m. pectoralis (protraction, depression)
m. subcoracoscapularis (anterior portion), m. deltoideus scapularis (both elevation, protraction)	m. coracobrachialis longus, m. coracobrachialis brevis, m. biceps, posterior portion of m. supracoracoideus (all retraction, depression)
m. subcoracoscapularis (posterior portion) (elevation, retraction)	anterior portion of m. supracoracoideus, m. deltoideus clavicularis (all depression, protraction)
m. latissimus dorsi, anterior portion of m. pectoralis, posterior portion of m. subcoracoscapularis, m. deltoideus scapularis, m. coracobrachialis brevis, m. coracobrachialis longus (rotation (leading edge upwards)	m. scapulohumeralis anterior, m. scapulohumeralis posterior, anterior portion of m. subcoracoscapularis, m. deltoideus clavicularis, posterior portion of m. pectoralis, m. biceps brachii, m. triceps brachii (leading edge downwards)
m. biceps (retraction, depression)	m. triceps (elevation, protraction)
m. extensor digitorum communis (extension metacarpals)	m. flexor digitorum longus (flexes digit I-V)
humeral triceps head (offsets ulna slightly dorsally), m. extensor carpi ulnaris (offsets ulna dorsally, or eventually extends metacarpal V)	m. flexor carpi ulnaris (displaces ulnar side of carpus ventrally, eventually flexes metacarpal V)
m. supinator longus and extensor carpi radialis (offsets radius or eventually the radial carpal side dorsally)	m. flexor carpi radialis (flexes metacarpal 1 or offsets the radial carpal side ventrally), m. pronator teres (offsets radius ventrally),

	m. brachialis (offsets radius slightly ventrally)

Table 3(on next page)

Agonistic and antagonistic femur muscles of *Cryptoclidus eurymerus* (IGPB R 324)

agonists	**antagonists**
m. puboischiofemoralis internus (pubis, vertebral column) (**protraction, elevation**)	m. puboischiofemoralis externus (ischium), m. adductor femoris, m. flexor tibialis internus (ischium), m. flexor tibialis externus (ischium), m. ischiotrochantericus, m. puboischiotibialis (retraction, depression)
m. puboischiofemoralis externus (pubis, anterior) (**protraction, and depression)**	m. puboischiofemoralis internus (ischium, ilium), m. caudifemoralis brevis and m. caudifemoralis longus, m. iliofibularis, m. iliotibialis, m. iliofemoralis, m. flexor tibialis externus (ilium), m. flexor tibialis internus (vertebral column) (retraction elevation)
m. ambiens (**protraction**), m. pubotibialis (**protraction**)	m. iliofibularis (elevation, retraction)
m. puboischiofemoralis externus (pubis), m. puboischiofemoralis internus (ischium, ilium), iliofemoralis, iliotibialis (rotates flipper leading edge up), m. ambiens and m. pubotibialis (rotates flipper leading edge up, if tibia below origin area),)	m. puboischiofemoralis externus (ischium), m. puboischiofemoralis internus (pubis), m. adductor femoris, m. ischiotrochantericus, m. flexor tibialis internus, m. caudifemoralis brevis, m. caudifemoralis longus, m. flexor tibialis externus, puboischiotibialis, m. iliofibularis (rotates flipper leading edge down), m. ambiens and m. pubotibialis (rotates flipper leading edge down, if tibia above origin area)
m. extensor digitorum longus (digital extensor), femorotibialis (offsets tibia dorsally)	m. gastrocnemius internus + m. gastrocnemius externus, m. flexor digitorum longus (digital flexors)

1

Table 4 (on next page)

Muscle forces of *Cryptoclidus eurymerus* (IGPB R 324) humerus by superposition of FESA load cases

muscle	muscle force [N]
m. supracoracoideus	6000
m. coracobrachialis brevis	4800
m. coracobrachialis longus	3600
m. deltoideus clavicularis	1500
m. deltoideus scapularis	1649
m. scapulohumeralis anterior	2400
m. scapulohumeralis posterior	1920
m. brachialis	324
m. triceps humeral head	275
m. pectoralis	9600
m. subcoracoscapularis	4422
m. latissimus dorsi	3918
m. extensor carpi ulnaris	1000
m. extensor digitorum communis	6000
m. extensor carpi radialis	1000
m. pronator teres	640
m. flexor carpi ulnaris	3000
m. flexor digitorum longus	1500
m. flexor carpi radialis	1500

Table 5(on next page)

Muscle forces of *Cryptoclidus eurymerus* (IGPB R 324) femur by superposition of FESA load cases

muscle	muscle force [N]
m. puboischiofemoralis externus	7878
m. puboischiofemoralis internus	7611
m. femorotibialis	1521
m. adductor femoris	3938
m. ischiotrochantericus	984
m. iliofemoralis	253
m. caudifemoralis brevis	506
m. caudifemoralis longus	507
m. extensor digitorum communis	1014
m. gastrocnemius	1176
m. flexor digitorum longus	786

Figure 1

Analog model demonstrating LOA of *Cryptoclidus eurymerus* (IGPB R 324) fore- and hindflipper.

Pectoral and pelvic girdle were fixed on a wooden frame. Thick styrofoam was placed into the glenoid and acetabulum joint cavity. Black threads helped to fix the flippers in their respective position. White threads represent LOA: a) screw eye pins were screwed into muscle attachment surfaces. Three electrical terminal strips were attached to one end. With hooks attached to each end of the thread, LOA were hung into the screw eye pins.

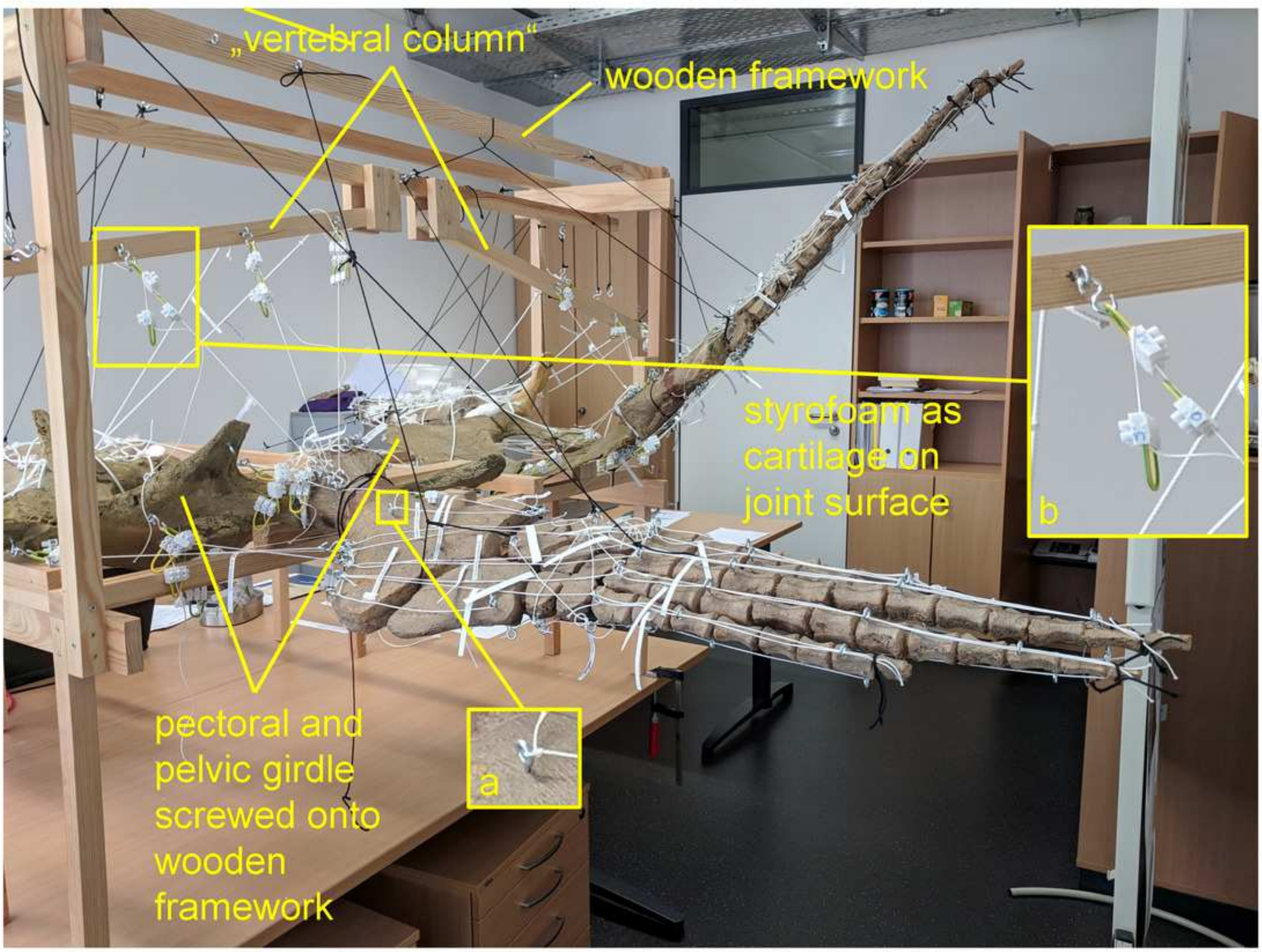

Figure 2

LOA of *Cryptoclidus eurymerus* (IGPB R 324) foreflipper in anterior and ventral view.

Pictures on the left (a, c, e, g) show an overview over all flipper muscles. Pictures on the right focus on the humerus muscles. a) and b) during maximum dorsal excursion in anterior view. c) and d) in the neutral position in anterior view. e) and f) during maximum ventral excursion in anterior view. g) and h) ventral view of the neutral foreflipper position. Abbreviations: b, Musculus brachialis; bb, Musculus biceps brachii; cb, Musculus coracobrachialis brevis; cl, Musculus coracobrachialis longus; dc, Musculus deltoideus clavicularis; ds, Musculus deltoideus scapularis; ecu, Musculus extensor carpi ulnaris; edc, Musculus extensor digitorum communis; fcr, Musculus flexor carpi radialis; fcu, Musculus flexor carpi ulnaris; fdlf, Musculus flexor digitorum longus (foreflipper); ld, Musculus latissimus dorsi; p, Musculus pectoralis; pte, Musculus pronator teres; sc, Musculus supracoracoideus; scs, Musculus subcoracoscapularis; shp, Musculus scapulohumeralis posterior; sl and ecr, Musculus supinator longus and Musculus extensor carpi radialis; tb, Musculus triceps brachii.

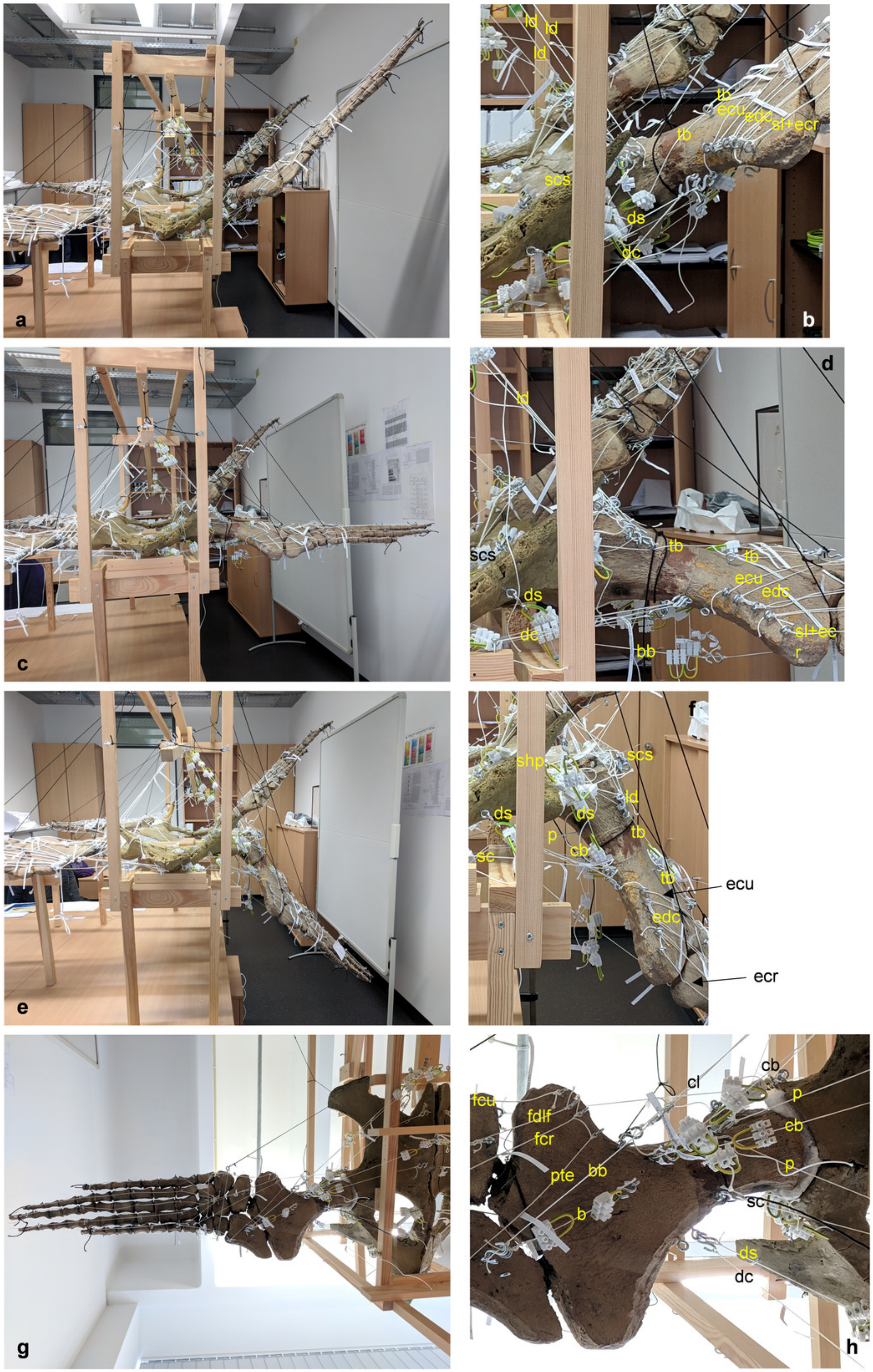
a
ld
ld
ld
tb
ecu
edc
sl+ecr
tb
scs
ds
dc
b
c
d
ld
scs
tb
tb
ecu
edc
ds
dc
sl+ec
r
bb
e
f
shp
scs
ld
ds
ds
p
tb
sc
cb
tb
ecu
edc
ecr
g
h
cl
cb
p
fcu
fdlf
cb
fcr
p
pte
bb
b
sc
ds
dc

Figure 3

LOA of *Cryptoclidus eurymerus* (IGPB R 324) foreflipper in posterior and dorsal view.

Pictures on the left (a, c, e, g) show an overview over all flipper muscles. Pictures on the right focus on the humerus muscles. a) and b) during maximum dorsal excursion in posterior view. c) and d) in the neutral position in posterior view. e) and f) during maximum ventral excursion in posterior view. g) and h) dorsal view of the neutral foreflipper position. Abbreviations: b, Musculus brachialis; bb, Musculus biceps brachii; cb, Musculus coracobrachialis brevis; cl, Musculus coracobrachialis longus; dc, Musculus deltoideus clavicularis; ds, Musculus deltoideus scapularis; ecu, Musculus extensor carpi ulnaris; edc, Musculus extensor digitorum communis; fcr, Musculus flexor carpi radialis; fcu, Musculus flexor carpi ulnaris; fdlf, Musculus flexor digitorum longus (foreflipper); ld, Musculus latissimus dorsi; pte, Musculus pronator teres; scs, Musculus subcoracoscapularis; shp, Musculus scapulohumeralis posterior; sl and ecr, Musculus supinator longus and Musculus extensor carpi radialis; tb, Musculus triceps brachii.

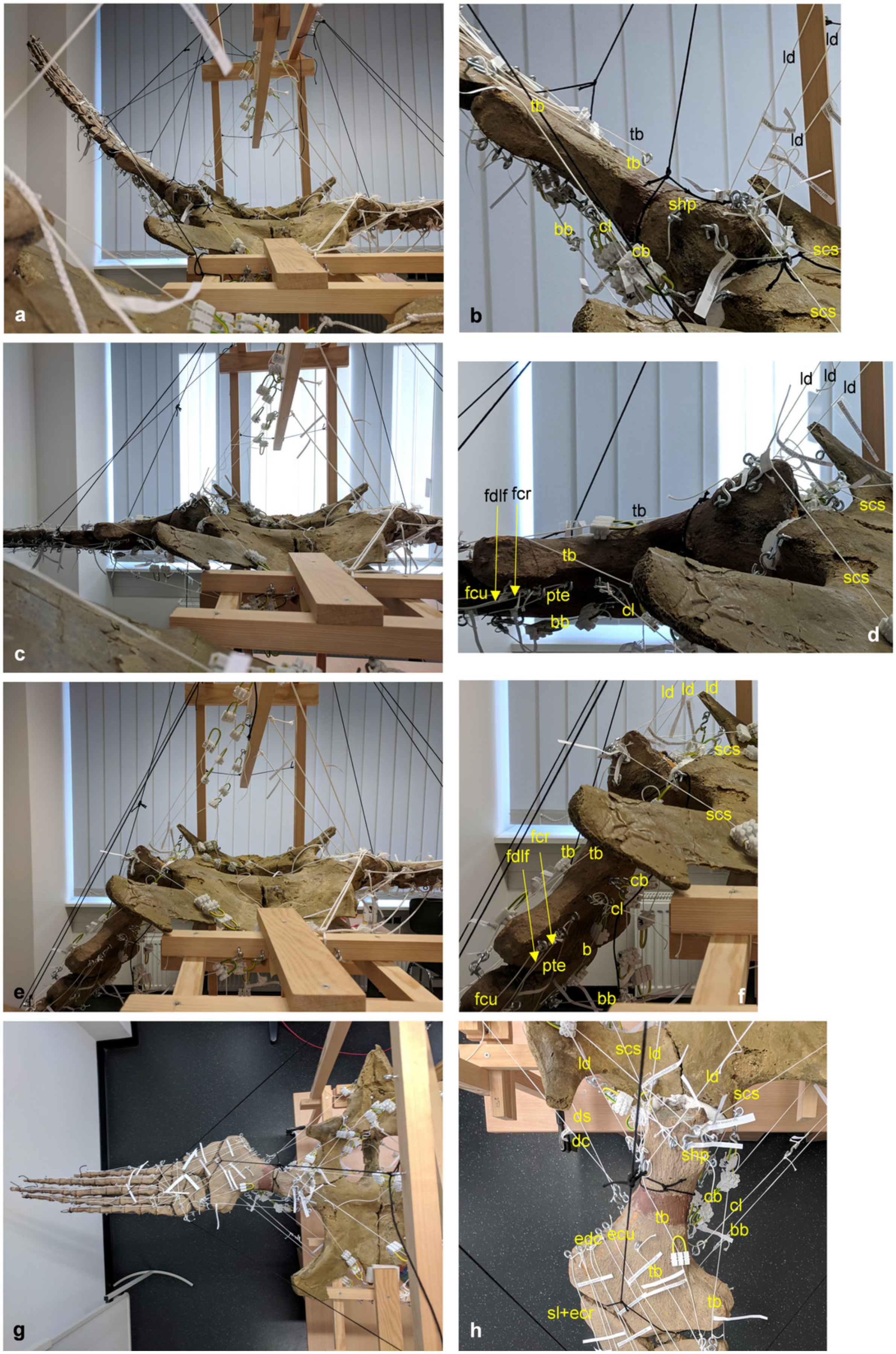
a
b
ld
ld
tb
tb
tb
ld
shp
bb
cl
cb
scs
scs
c
d
ld
ld
ld
fdlf
fcr
tb
scs
tb
scs
fcu
pte
cl
bb
e
f
ld
ld
ld
scs
scs
fcr
fdlf
tb
tb
cb
cl
b
pte
fcu
bb
g
h
scs
ld
ld
ld
scs
ds
dc
shp
cb
cl
tb
bb
edc
ecu
tb
sl+ecr
tb

Figure 4

LOA of *Cryptoclidus eurymerus* (IGPB R 324) hindflipper in anterior and ventral view.

Pictures on the left (a, c, e, g) show an overview over all flipper muscles. Pictures on the right focus on the femur muscles. a) and b) during maximum dorsal excursion in anterior view. c) and d) in the neutral position in anterior view. e) and f) during maximum ventral excursion in anterior view. g) and h) ventral view of the neutral hindflipper position. Abbreviations: a, Musculus ambiens; af, Musculus adductor femoris; cfb, Musculus caudifemoralis brevis; cfl, Musculus caudifemoralis longus; edl, Musculus extensor digitorum longus; f, Musculus femorotibialis; fdlh, Musculus flexor digitorum longus (hindflipper); fte, Musculus flexor tibialis externus; fti, Musculus flexor tibialis internus; gi and ge, Musculus gastrocnemius internus and Musculus gastrocnemius externus; i, Musculus ischiotrochantericus; ife, Musculus iliofemoralis; ifi, Musculus iliofibularis; it, Musculus iliotibialis; pe, Musculus puboischiofemoralis externus; pi, Musculus puboischiofemoralis internus; pit, Musculus puboischiotibialis; pti, Musculus pubotibialis.


a
b
ifi
pi
edl
f
it
fti
fte
cfb+cfl
ife
a
pit
pti
c
d
e
f
ifi
it
ife
g
h
pe
gi+ge
pti
pit
af
fdlh
fte
fti
i
cfb+cfl

Figure 5

LOA of *Cryptoclidus eurymerus* (IGPB R 324) hindflipper in posterior and dorsal view.

Pictures on the left (a, c, e, g) show an overview over all flipper muscles. Pictures on the right focus on the femur muscles. a) and b) during maximum dorsal excursion in posterior view. c) and d) in the neutral position in posterior view. e) and f) during maximum ventral excursion in posterior view. g) and h) dorsal view of the neutral hindflipper position. Abbreviations: a, Musculus ambiens; af, Musculus adductor femoris; cfb, Musculus caudifemoralis brevis; cfl, Musculus caudifemoralis longus; edl, Musculus extensor digitorum longus; f, Musculus femorotibialis; fte, Musculus flexor tibialis externus; fti, Musculus flexor tibialis internus; i, Musculus ischiotrochantericus; ife, Musculus iliofemoralis; ifi, Musculus iliofibularis; it, Musculus iliotibialis; pe, Musculus puboischiofemoralis externus; pi, Musculus puboischiofemoralis internus; pit, Musculus puboischiotibialis; pti, Musculus pubotibialis.

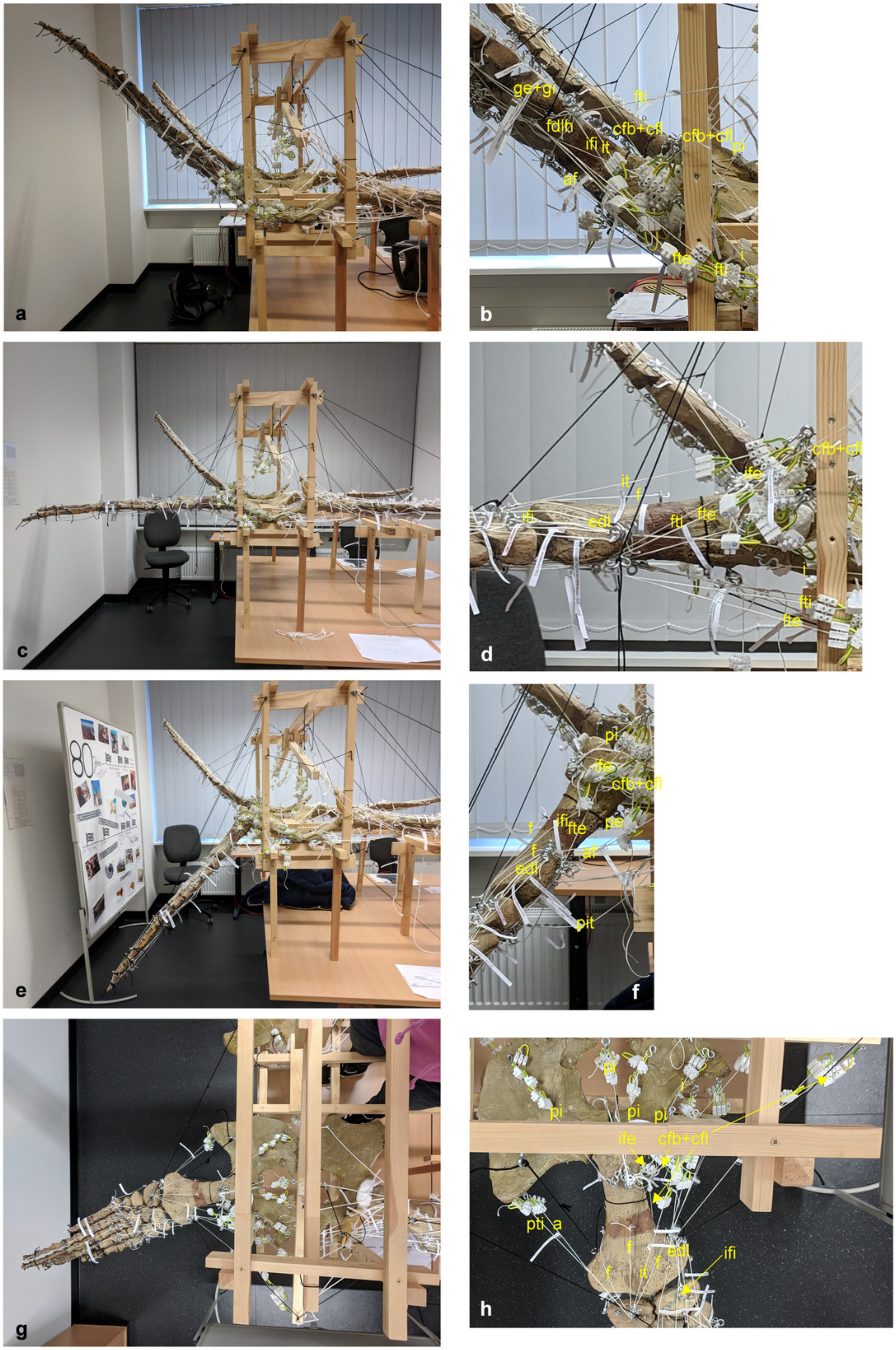
a
b
ge+gi
fti
fdlh
cfb+cfl
cfb+cfl
ifi
it
pi
af
fte
fti
i
c
d
cfb+cfl
ife
it
f
ifi
edl
fti
fte
i
fti
fte
e
f
pi
ife
cfb+cfl
f
ifi
fte
pe
f
af
edl
pit
g
h
pi
pi
pi
pi
ife
cfb+cfl
pti
a
f
edl
ifi
f
it
f

Figure 6

Total length change of muscles. a) humerus muscle(s) (portions) and b) femur muscle(s) (portions).

a) and **b)** Locomotory muscles that insert into or originate from humerus and femur cover the whole spectrum of maximum total muscle length change of vertebrate muscle well, ranging from no measurable total length change (of muscles with a complex architecture) to around 40% of total length change of muscle (typical for approximately parallel-fibred muscles; marked by turquoise line) (Biewener, Corning & Tobalske, 1998; Biewener & Roberts, 2000). **N**ote in a) how m. deltoideus scapularis (1), if it originates from the scapula, would show an unphysiological total length change of muscle. If it originates from the ventral scapula (2), total muscle length change drops down into the physiological spectrum and ranges within the measuring error (typical for muscles with a complex internal architecture).

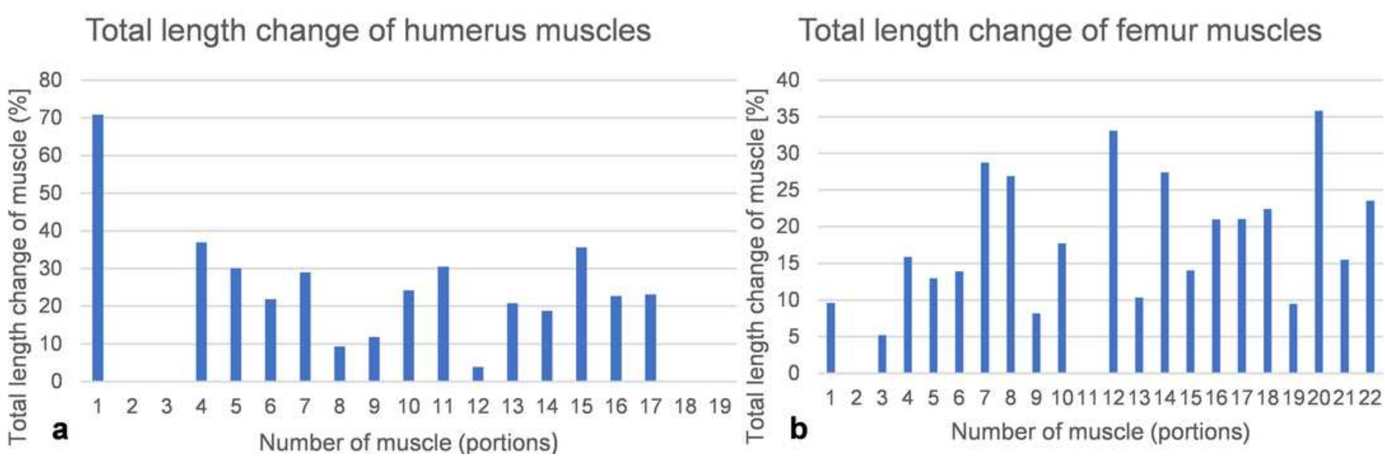

Figure 7

FESA of *Cryptoclidus eurymerus* (IGPB R 324) humerus and femur. a)-d) humerus, e)-h) femur.

a), **e)** contour drawings of humerus and femur and lines of action of the respective muscles in ventral view which were derived by spanning threads into the flipper skeleton of *Cryptoclidus*. **b) f)** meshed volumetric FE models with force vectors in ventral view which were transferred from the contour drawings (a, e). FESA superpositions of both load cases (down- and upstroke) in **c)**, **d)** in dorsoventral view and **g)**, **h)** in anteroposterior view. The colour spectrum codes the compressive stress in MPa. Please note how regions of lower compressive stress match with regions of spongy bone and regions of higher compressive stress match with cortical bone. Abbreviations: af, Musculus adductor femoris; b, Musculus brachialis; bb, Musculus biceps brachii; cb, Musculus coracobrachialis brevis; cfb, Musculus caudifemoralis brevis; cfl, Musculus caudifemoralis longus; cl, Musculus coracobrachialis longus; dc, Musculus deltoideus clavicularis; ds, Musculus deltoideus scapularis; f, Musculus femorotibialis; fcr, Musculus flexor carpi radialis; fcu, Musculus flexor carpi ulnaris; fdlf, Musculus flexor digitorum longus (foreflipper); fdlh, Musculus flexor digitorum longus (hindflipper); fte, Musculus flexor tibialis externus; fti, Musculus flexor tibialis internus; gi and ge, Musculus gastrocnemius internus and Musculus gastrocnemius externus; i, Musculus ischiotrochantericus; p, Musculus pectoralis; pe, Musculus puboischiofemoralis externus; pit, Musculus puboischiotibialis; pte, Musculus pronator teres; pti, Musculus pubotibialis; sc, Musculus supracoracoideus.

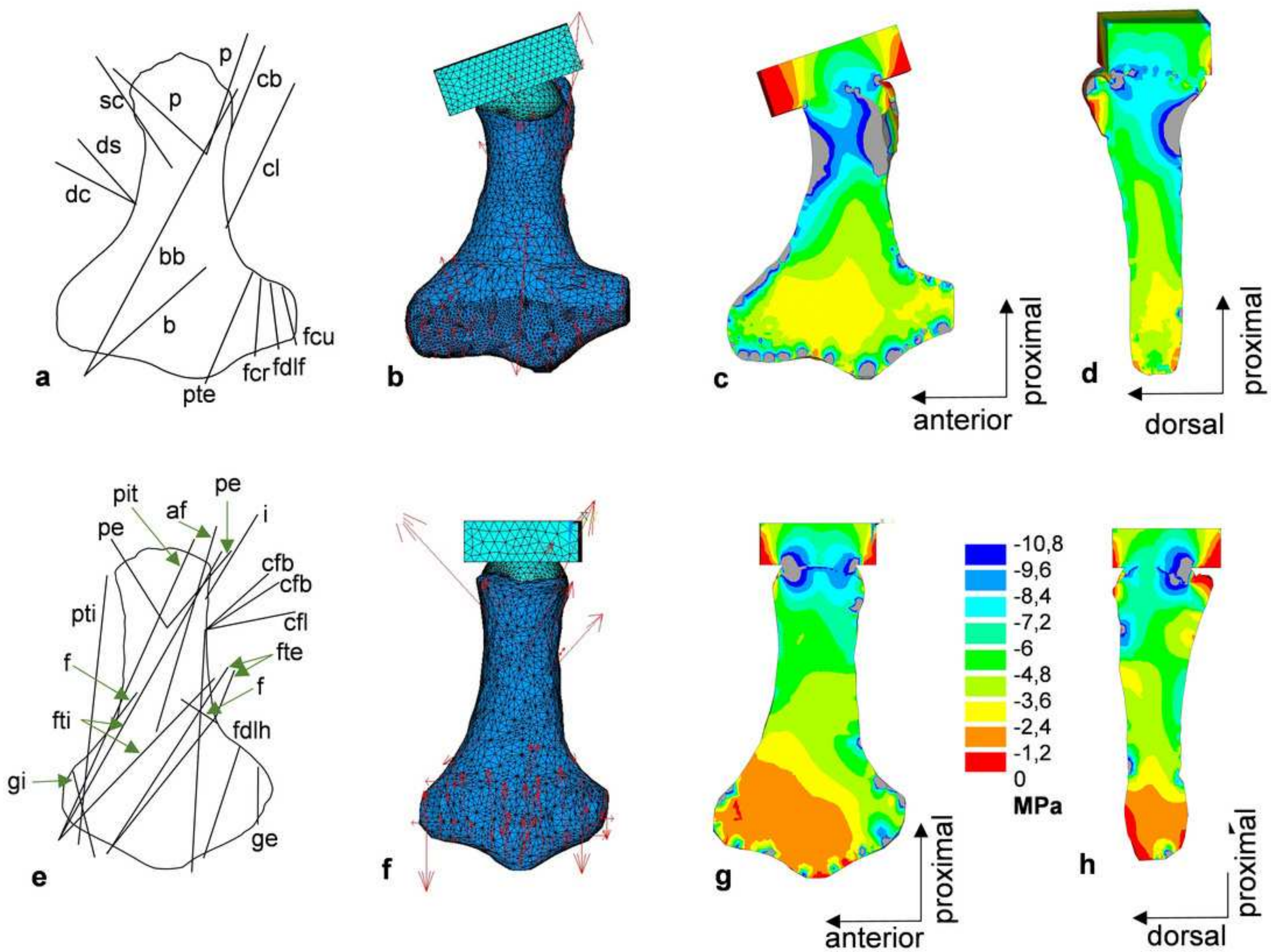
p
sc
p
cb
ds
cl
dc
bb
b
fcu
fcr
fdlf
pte
proximal
anterior
proximal
dorsal
pit
pe
af
pe
i
cfb
cfb
pti
cfl
fte
f
f
fti
fdlh
gi
ge
-10,8
-9,6
-8,4
-7,2
-6
-4,8
-3,6
-2,4
-1,2
0
MPa
proximal
anterior
proximal
dorsal
a
b
c
d
e
f
g
h